PATTERNED SINGLE-WALLED CARBON NANOTUBE NETWORKS FOR NANOELECTRONIC DEVICES

By

Yingduo Chen
B. Eng, Huazhong University of Science and Technology, China, 2009

A Dissertation Submitted in Partial Fulfillment
of the Requirements for the Degree of

MASTER OF APPLIED SCIENCE

in the Department of Electrical and Computer Engineering

SUPERVISORY COMMITTEE

PATTERNED SINGLED-WALLED CARBON NANOTUBE NETWORKS FOR NANOELECTRONIC DEVICES

by

Yingduo Chen
B. Eng, Huazhong University of Science and Technology, China, 2009

Supervisory Committee

Dr. Chris Papadopoulos, (Department of Electrical and Computer Engineering)
Supervisor

Dr. Tao Lu, (Department of Electrical and Computer Engineering)

ABSTRACT

Dr. Chris Papadopoulos, (Department of Electrical and Computer Engineering)
Supervisor

Dr. Tao Lu, (Department of Electrical and Computer Engineering)

Single-walled carbon nanotubes (SWNTs), with their superior combination of electrical and mechanical properties, have drawn attention from many researchers for potential applications in electronics. Many SWNT-based electronic device prototypes have been developed including transistors, interconnects and flexible electronics. In this thesis, a fabrication method for patterned SWNT networks and devices based on colloidal lithography is presented. Patterned SWNT networks are for the first time formed via solution deposition on a heterogeneous surface. This method demonstrates a simple and straight-forward way to fabricate SWNT networks in a controllable manner.

Colloidal sphere monolayers were obtained by drop-casting from solution onto clean substrates. The colloidal monolayer was utilized as a mask for the fabrication of patterned SWNT networks. SWNT networks were shown to be patterned either by depositing SWNT solutions on top of a colloidal monolayer or by depositing a mixed SWNT-colloidal sphere aqueous suspension on the substrates. Colloidal monolayers were examined by optical microscopy and it was found that the monolayer quality can be affected by the concentration of colloids in solution. Polystyrene colloidal solution with concentration of 0.02 wt% ~ 0.04 wt % was found optimal for maximum coverage of colloidal monolayers on SiO_2 substrates. After removing the colloidal spheres, the topology of the patterned SWNT networks was characterized by atomic force microscopy and scanning electron

microscopy. Two-dimensional ordered arrays of SWNT rings and SWNTs interconnecting the SWNT rings were observed in the resulting network structure. The height of the rings was about 4-10 nm and the diameter was about 400 nm. In some samples, mesh-like patterned SWNT networks are also observed. It is hypothesized that the capillary forces induced by Van der Waals interaction at liquid/air/solid interfaces play an important role during the formation of the patterned SWNT networks. Raman spectroscopy was also employed to identify the chirality and diameter of the SWNTs in the networks. Both metallic and semiconducting SWNTs were found in the networks and the diameter of the SWNTs was about 1 to 2 nm.

The electrical properties of SWNT networks, including random SWNT networks, partially patterned SWNT networks and fully patterned SWNT networks were characterized by a probe station and a Keithley 4200 semiconductor measurement system. The random SWNT networks had two-terminal resistance varying between several MΩ to several hundred MΩ. Field effect behavior was observed in some devices with relatively high resistance and nonlinear I-V curves. Those devices had on/off ratio of less than 100. There was significant leakage current in the "off" state likely due to metallic tube pathways in the networks. The partially patterned SWNT networks had resistance that varied from 20 KΩ to 10 MΩ, but did not display field effect behavior in our studies.

The resistance of the patterned SWNT networks was about 10 MΩ - 100 MΩ. The electrical characteristics of the patterned SWNT networks as thin film transistors were investigated, and the on/off ratio of the devices varied from 3 to 10^5. The upper limit of mobility in the devices was about ~ 0.71 – 5 $cm^2/V \cdot s$. The subthreshold slope of patterned SWNT network FETs can be as low as 210 meV/dec.

TABLE OF CONTENTS

LIST OF FIGURES

LIST OF TABLES

ACKNOWLEDGEMENTS

I would like to thank:

My supervisor Dr. Chris Papadopoulos, for his guidance through this work. This thesis is impossible to be finished without his supervision and valuable suggestions.

Dr. Tao Lu for their kindly guidance as my thesis committee members.

Jian Dong, my girlfriend for her support and inspiration.

My friends, Daniel Cai, Jun Zhu, Bojiang Ma, Ji Huang, Wenhao Jin, Carl Zhang, Sara Zhang, Edison Guo, Yimian Du, Liya Zhu, Xiaohe Fan, Zhiguang Wang, Di Wang, for bringing me happiness and courage in life.

My parents, my aunt and uncle and other family members for their love and support

1 INTRODUCTION

Carbon nanotubes (CNTs) are allotropes of carbon with one-dimensional (1-D) cylindrical structure. CNTs can be categorized into two groups – multi-walled carbon nanotubes (MWNTs) and single-walled carbon nanotubes (SWNTs), as shown in Figure 1. Normally MWNTs comprise multiple concentric tubes with diameter of 2 ~ 50 nm and length of 5 ~ 50 μm. In contrast, SWNTs have single-layer tube structures with diameter of at most a few nanometers and length of several hundred nanometers to several micrometers.

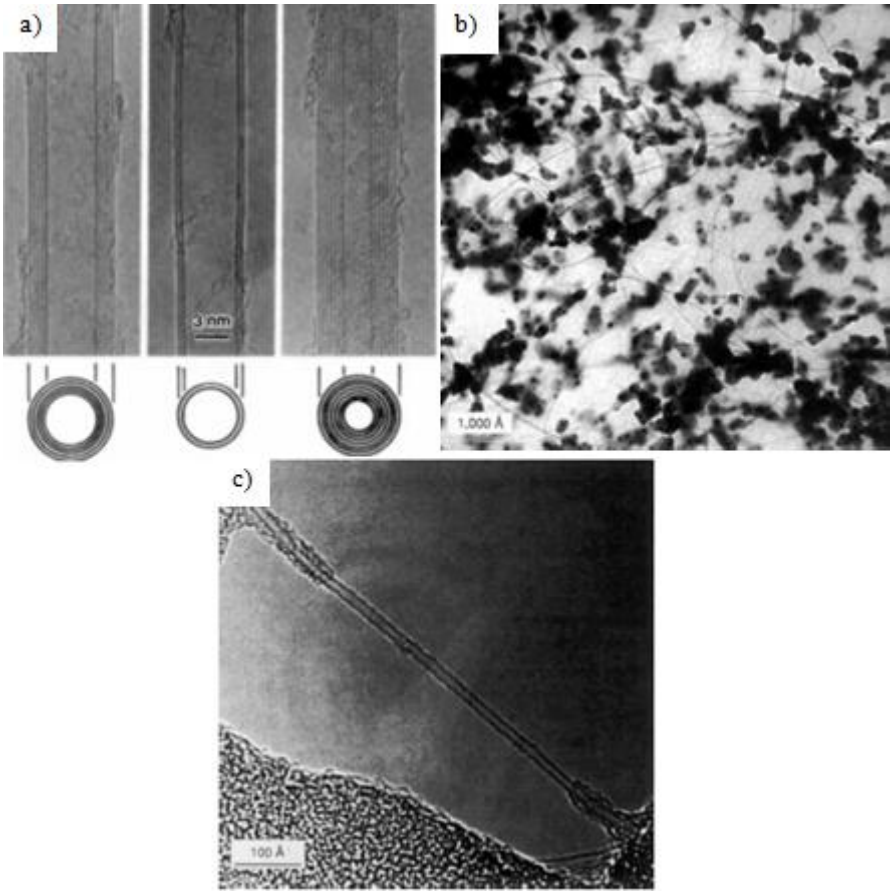

Figure 1: a) TEM (transmission electron microscopy) images of multi-walled carbon nanotubes [1]; b) TEM image of SWNT bundles containing cobalt catalyst and SWNTs; c) TEM image of an individual SWNT [2].

Since the discovery of CNTs in 1991 by Iijima [1], many interesting properties of carbon nanotubes have been revealed, including high strength and flexibility, large electronic and thermal conductivity. MWNTs have been commercially used in various structural materials as additives for strength-enhancing purposes [3]. Besides their superior mechanical properties, carbon nanotubes also show ultra-high thermal conductivity of > 3000 $W/(m \cdot K)$ which is five times higher than that of copper [4]. In addition, the electrical conductivity of carbon nanotubes is comparable to copper. Therefore, the high thermal and electrical conductivity makes CNTs promising candidates for electrical applications, such as conducting wires, electrode materials and active electronic devices.

CNTs are also widely studied as active materials in energy storage applications due to their chemical stability and high electrical conductivity. For example, CNTs as electrode materials of supercapacitors and Li-ion batteries can significantly increase their energy capacity [5, 6]. In organic solar cells, conjugated polymers with percolating CNT networks can enhance the charge separation and electron conductivity [7]. In fuel cell systems, CNTs replacing carbon blacks as supporting materials for Pt catalyst can achieve an increased utilization efficiency of platinum catalyst and thus lead to cost reduction [8].

SWNTs are considered promising materials for electronic applications, due to their nanoscale dimensions and exceptional electrical properties. Depending on their chirality, SWNTs can be either metallic or semiconducting. In metallic tubes, electrons can transport ballistically at room temperature with minimal scattering [9, 10]. Metallic SWNTs can carry current of ~ 25 μA per tube that is comparable to the best conductors available. Therefore, metallic tubes can replace copper as interconnects in integrated circuits in order to improve current carrying capacity [11]. Semiconducting SWNTs are attractive for

transistor applications because of their high carrier mobility exceeding $100000\,cm^2/V\cdot s$ and their compatibilities with silicon transistor architecture [12]. It is predicted that the feature size of transistors with semiconducting SWNT channels can be scaled down to several nanometers without any performance degradation [13]. Since silicon-based field effect transistors (Si-FETs) face adverse short-channel effects when the channel length shrinks to sub-10 nm, semiconducting SWNTs will be a promising alternative for continuing miniaturization of transistor devices and Moore's Law. Due to their superb mechanical and optical properties, SWNTs can also be promising materials for flexible and transparent electronics which have wide applications in optical display as well as biological industries [14].

The application of SWNTs is currently limited by the difficulties of fabrication capability, especially for devices based on individual SWNTs. Two-dimensional networks of single-walled carbon nanotubes (SWNTs), as an ensemble of individual SWNTs, are however relatively simple to fabricate. But it is very challenging to obtain a large quantity of individual SWNTs with consistent properties. Therefore, the fabrication, properties and applications of SWNT networks are being intensively investigated. A great deal of electronic device prototypes based on SWNT networks have been demonstrated, such as field effect transistors [15, 16], chemical and biological sensors [17, 18], flexible and transparent electronics [19, 20].

SWNT networks can be fabricated either by depositing the SWNTs from solution or by direct growth via chemical vapor deposition (CVD). Since the morphology of SWNT networks determines its physical properties, it is important to fabricate SWNT networks with well-defined structures.

In this work, a fabrication method of patterning nanotube networks is investigated. An ordered SWNT structure can be realized by depositing carbon nanotubes on colloidal sphere monolayer masks. This simple and straight-forward fabrication process can be done readily at room temperature in an ambient environment.

1.1 The Structure of Single-Walled Carbon Nanotubes (SWNTs)

A single-walled carbon nanotube (SWNT) is a unique one-dimensional nanomaterial, which consists of a graphene sheet rolled up to a seamless hollow cylinder, as shown in Figure 2. The diameter of a SWNT is about 0.7 to 2 nm, and its length is typically several micrometres up to several centimetres long.

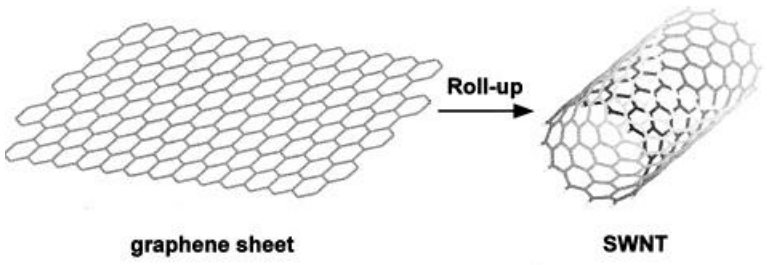

Figure 2: A schematic view of the formation of a SWNT by rolling up a graphene sheet [21].

The carbon atoms on a graphene sheet are arranged in a hexagonal lattice. Depending on the direction that graphene is rolled, the SWNTs are categorized into three groups: zigzag, armchair and chiral. As shown in Figure 3, the atomic structure of SWNTs is characterized by the chiral vector $\vec{C}_h = n\vec{a}_1 + m\vec{a}_2$. The integers (n, m) are defined as their helicity. The unit vector of SWNTs is described as the translation vector $\vec{T}$ which is normal to the chiral vector $\vec{C}_h$. If n=m or $\vec{C}_h = (n, n)$, the SWNTs have so-called armchair structures. If m=0 or

n=0 or $\vec{C}_h$ =(n,0) , the SWNTs have zigzag structures. All the rest of the nanotubes belong to the chiral class. Examples of all three types of SWNTs are shown in Figure 4. The chirality of the SWNTs determines the diameter d_t by the equation $d_t = \frac{a}{\pi}\sqrt{n^2+m^2+n\cdot m}$ in which the lattice constant a = 1.44 Å × $\sqrt{3}$ = 2.49 Å [22]. The structure of SWNTs determines their fundamental electronic properties.

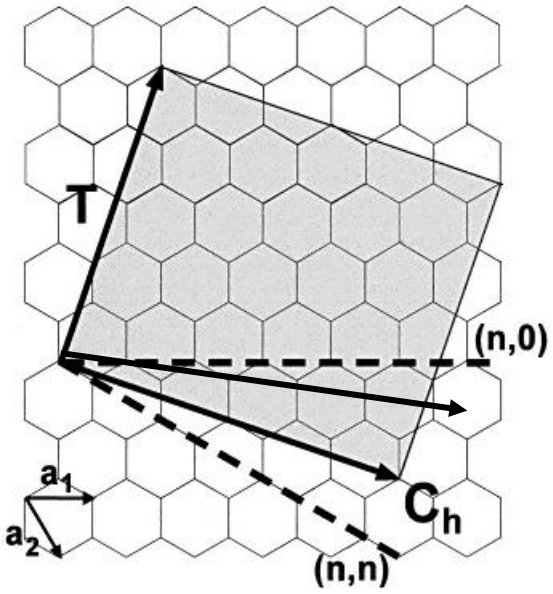

Figure 3: Schematic of unrolled nanotube lattice. $\vec{a}_1$ **and** $\vec{a}_2$ **are lattice vectors.** $\vec{C}_k = n\vec{a}_1 + m\vec{a}_2$ **is the roll-up vector, in which the integers** (n,m) **define the helicity.**

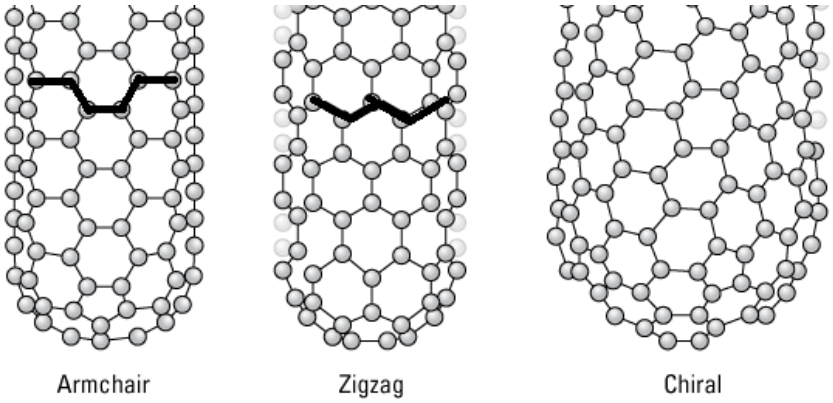

Figure 4: Examples of the three types of SWNTs: armchair, zigzag and chiral [23].

1.2 Electronic Structure of Graphene and SWNTs

SWNTs can be either metallic or semiconducting depending on their chiral vector (n, m) [24, 25]. SWNTs are metallic when n-m=3l and semiconducting when n-m≠3l (l is integer). Statistically, as-grown SWNTs have 1/3 metallic nanotubes and 2/3 semiconducting nanotubes.

To understand the electronic properties of SWNTs, the bandstructure of π electrons in graphene needs to be analyzed. One simple approach to calculate the bandstructure of π electrons is using the tight binding model which considers only the nearest neighbor interactions of the lattice. The energy dispersion of the π^*-π band can be described in this case as the following equation [26, 27]:

$$E_{2D}(k_x, k_y) = \pm\gamma_0[1 + 4\cos\left(\frac{\sqrt{3}k_x a}{2}\right)\cos\left(\frac{k_y a}{2}\right) + 4\cos^2\left(\frac{k_y a}{2}\right)])]$$

where γ_0 is the nearest-neighbor transfer integral, k_x and k_y are the wave vectors along the x, y direction and a is the length of the C-C bond.

The band structure of π electrons in 2D graphene is shown in Figure 5a). The most interesting finding of this bandstructure profile is that the π^* and π bands are degenerate at six points, known as K points in the first Brillouin zone. Therefore, graphene is defined as a zero-bandgap semiconductor.

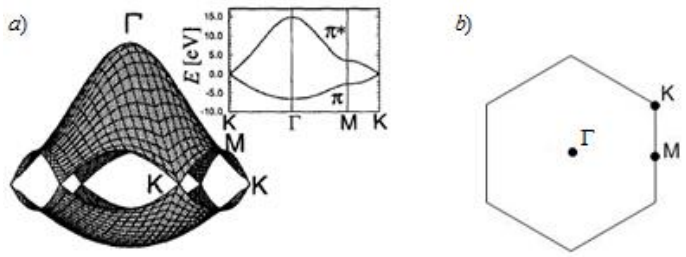

Figure 5: a) Band structure of graphene π-band for the first Brillouin zone [26]; b) The first Brillouin zone showing high symmetry points Γ, M, K.

The bandstructure of SWNTs can be derived from the bandstructure of graphene. Since SWNTs can be seen as a rolled-up graphene sheet, the wavefunction of the electrons in the SWNTs is similar to the electrons in graphene but with periodic boundary conditions in the circumferential direction. Given a SWNT with indices (n,m), it is rolled up by the chiral vector $\vec{C}_h = n\vec{a}_1 + m\vec{a}_2$. According to Bloch's theorem, the wavefunction of the electrons in the graphene can be expressed as $\psi(\vec{R}) = e^{i\vec{K}\cdot\vec{R}} u(\vec{R})$, where u is a function with the lattice periodicity. By applying periodic boundary conditions to this equation, the wavefunction of the electrons in SWNTs can be expressed as $\psi(0) = \psi(n\vec{a}_1 + m\vec{a}_2)$. Thus the allowed wave vector $\vec{k}$ in SWNTs is quantized and it can be derived from the following periodic boundary condition $\vec{C}_h \cdot \vec{k} = 2\pi j$ (j is integer).

Therefore only a discrete number of the wave vectors along the circumferential direction are allowed in SWNTs. The bandstructure of SWNTs thus consists of a group of one-

dimensional sub-bands which can be seen as a series of cross-section profiles of the bandstructure of graphene. As shown in Figure 6, if one of the sub-bands passes through a K point (Figure 6a)), the SWNT is metallic tubes with zero-bandgap. If none of the sub-bands come across the K point, the SWNTs are semiconducting with finite bandgap (Figure 6b)). The chiral indices (n,m) of a SWNT determine whether the SWNTs are metallic or semiconducting: the SWNT is metallic if (n-m) is a multiple of 3, otherwise, the tube is semiconducting [26].

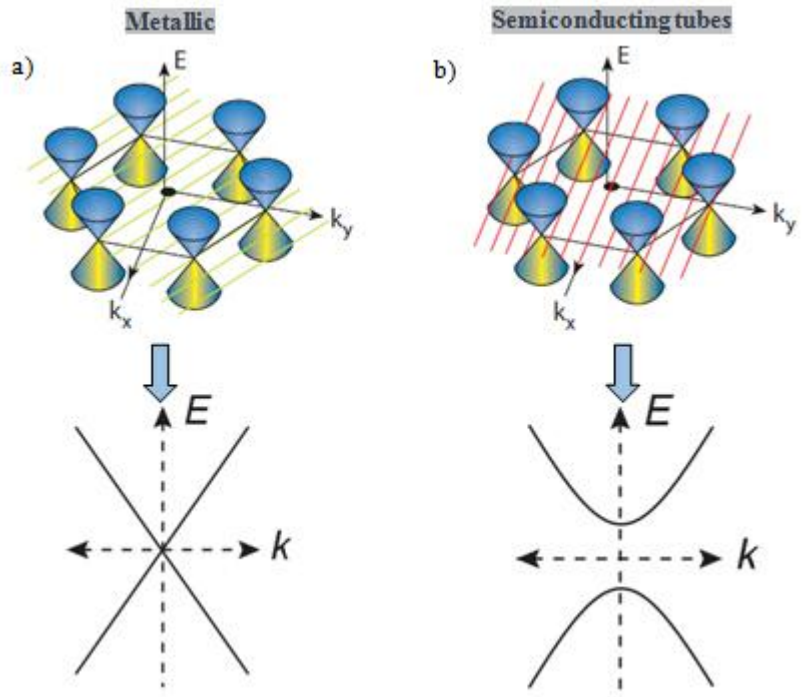

Figure 6: Band structure of metallic and semiconducting SWNTs [28]. a): Metallic tubes with zero-bandgap; b): Semiconducting tubes with finite bandgaps.

The electronic transport properties of individual SWNTs are of great interest to the academic community and are being thoroughly investigated. Under ideal conditions, metallic SWNTs have been revealed to be ballistic conductors (no scattering) [10, 29]. The

conductance of semiconducting SWNTs is normally a few percent of the quantum ballistic conductance limit $4e^2/h$. The lower conductance of semiconducting SWNTs is caused by the Schottky barriers formed at metal-tube contacts. It is also found that semiconducting SWNTs can form low resistive Ohmic contacts with certain metals, such as Pd and the conductance of semiconducting SWNTs can reach up to $(0.4\sim0.5)\times4e^2/h$ [10].

However, structural disorders in the SWNTs such as localized lattice defects, electrostatic potential fluctuations and mechanical deformation can cause electron scattering in the conductance channel and negatively affect the conductance of SWNTs [30]. There are two different types of backscattering in the electronic transport caused by structural disorders – long-range disorders and short-range disorders. The metallic SWNTs can be only affected by short-range disorder because of the symmetries of electronic wave-function [31]. However, semiconducting SWNTs are subject to both long-range and short-range disorders [32, 33]. Therefore metallic SWNTs have long mean free path at micrometer scale, whereas the mean free path of semiconducting SWNTs is at the hundreds of nanometre level [33].

Other than the structural disorder in SWNTs, electron-phonon scattering is another important process to be considered in the electronic transport of SWNTs. It has been observed that acoustic phonons are dominant at low bias voltage with the mean free path ranging from several hundreds of nm to several μm [34].

1.3 Electrical Properties of Graphene/SWNT Field Effect Transistors

A field effect transistor (FET) is a type of device that uses electrical fields to control the conductivity of semiconducting channels. A typical FET consists of a channel, a gate electrode and source/drain electrodes (Figure 7). Currently, silicon-based FETs are the standard, widely used for microprocessors and memory chips. The performance enhancement of silicon-based devices are driven by the scaling of its physical dimensions, as described by Moore's Law stating that the density of transistors in integrated circuits is doubled every 18 to 24 months. However, the minimum feature size of transistors is currently approaching the regime of 10 nm where adverse short-channel effects can negatively impact the performance improvement of nanoscale silicon devices [35].

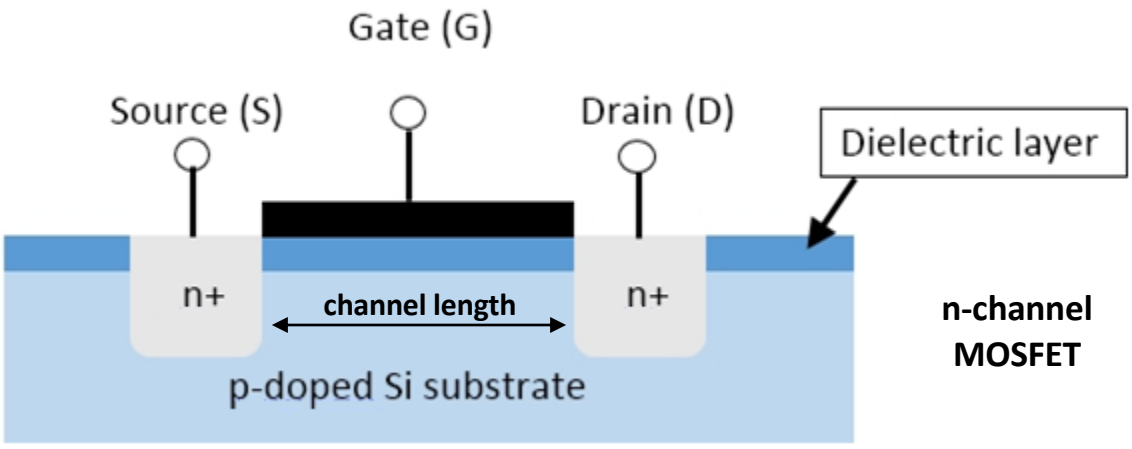

Figure 7: Schematic of a typical n-channel MOSFET [36]

Because of the defect-free 2-D structure, the charge carriers in graphene can transport over long distance (up to several micrometers) without significant scattering. The intrinsic mobility of graphene can reach over 200000 $cm^2/V \cdot s$ which is two orders of magnitude

higher than the mobility of silicon [37, 38]. However, graphene has a gapless bandstructure that causes on/off ratio of < 10 in graphene transistors. In order to create a bandgap in graphene, various methods have been introduced. For example, bandgap can be introduced in bilayer graphene by applying electric field upon the graphene layers. This is because of the introduction of symmetry breaking in graphene layer by external electrical field [39, 40]. Applying an uniaxial strain on graphene can also create bandgaps [41, 42]. This is due to the breaking of equivalence of sublattices. Similarly, the bandgap is also observed in graphene sheet that is epitaxially grown on SiC substrates. In this case, the substrate asymmetry causes the formation of a bandgap [43, 44].

The bandgap in graphene sheet can also be induced by reducing its width. The bandgap can be created in graphene when the width of graphene sheet is reduced to 100 nm or narrower. Graphene sheets with narrow width are often called graphene nanoribbon (GNRs). In GNRs, the carriers are confined to a quasi-one-dimensional channel and thus a bandgap is opened up near the Dirac points (Dirac points are the six corners of the Brillouin zone in graphene bandstructure). The size of bandgap is found to be inversely proportional to the width of GNRs.

GNRs can be obtained by various methods such as via lithography, unzipping CNTs, and epitaxial growth. The width of GNRs obtained by e-beam lithography can be as narrow as 20 nm. However, structural defects and significant width variation introduced in the fabrication process can deteriorate the electronic properties of GNRs via e-beam lithography [45-47]. GNRs with width 2.5 nm can be fabricated by scanning tunneling lithography (STL) [48]. The bandgap of ultra-narrow GNRs can be up to 0.5 eV. By unzipping SWNTs or directly growth, GNRs with width of a few nm can be obtained [49].

With the introduction of bandgap in GNRs, transistors using GNRs as channel materials have been developed and extensively studied. For example, a lithographically patterned GNR with width of 24 nm showed 100 meV bandgap and on/off ratio of 10 [50]. In one report, a transistor based on a sub-10 nm GNR have achieved on/off ratio of 10^5 at room temperature [51, 52]. However, the mobility of the device is ~100-200 $cm^2/V \cdot s$, which is lower than that of graphene sheet. This is due to the introduction of defects and bandgap causing mobility degradation. The effective mass of carriers increases when the bandgap of the GNRs gets larger.

Compared to graphene, semiconducting SWNTs have an intrinsic bandgap making it favorable for transistor applications. CNTFETs using semiconducting CNTs as conducting channel can avoid short-channel effects, due to the efficient electrostatic control over the ultrathin body of SWNT channel [13, 53]. The first CNTFETs were fabricated in 1998 independently by two groups --- IBM and TU Delft [54, 55]. The schematics of the first two CNTFETs and their output characteristics are shown in Figure 8. Both devices used heavily doped silicon as backgate and thermally grown silicon oxide as the dielectric layer. Gold and platinum were used as electrodes by IBM and TU Delft, respectively. Results of electrical measurements showed that both CNTFETs were p-type transistors which can be completely turned off at positive gate bias. The on/off ratio of both devices was more than five orders of magnitude.

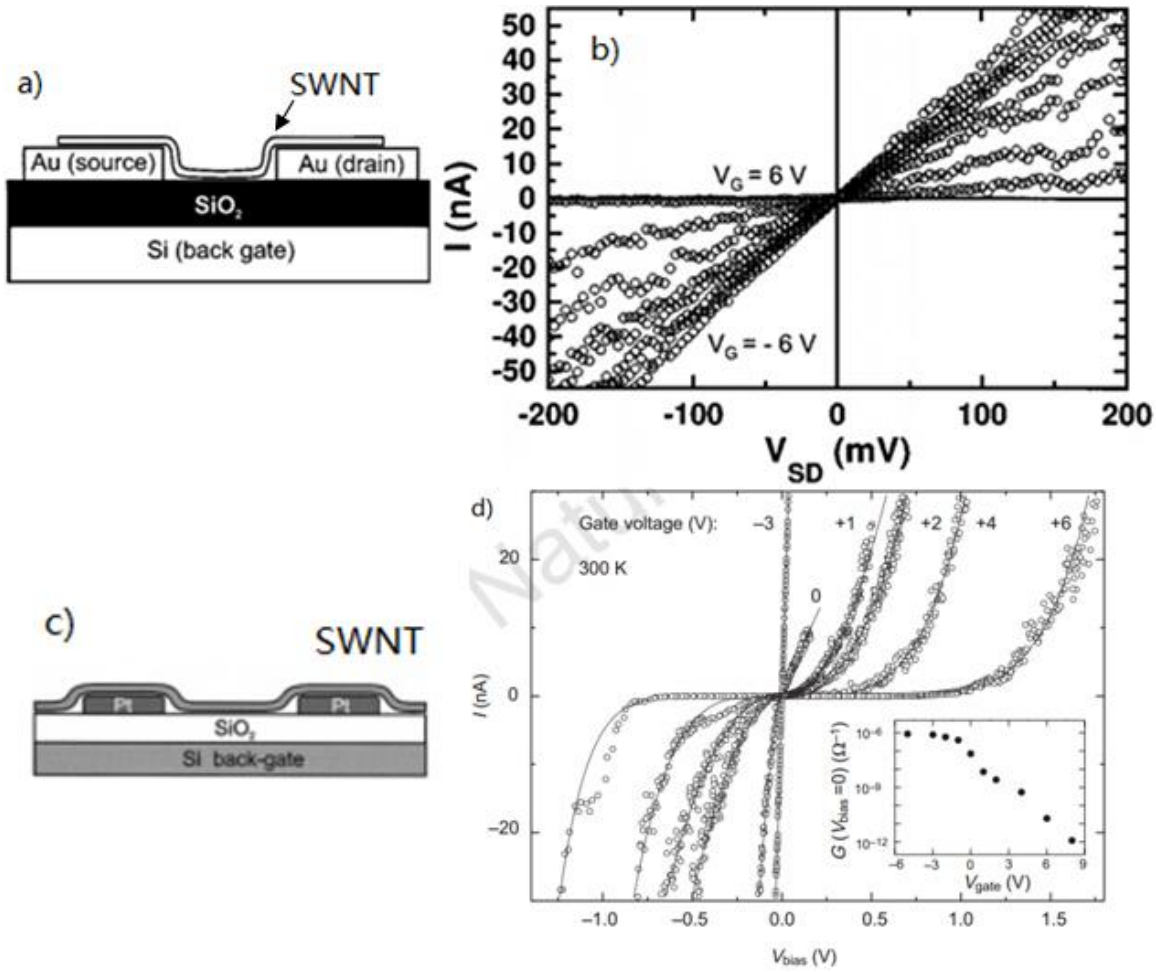

Figure 8: Schematic of CNTFET developed by IBM (a) and its output characteristics (b); Schematic of CNTFET developed by TU Delft (c) and its output characteristics (d).

Similar to other kinds of transistor devices, the performance of CNTFETs can be assessed by a few key parameters including current carrying capability, on/off ratio, subthreshold slope, transconductance and carrier mobility. The superior electrical properties of SWNTs make CNTFETs outperform silicon transistors in many aspects [10].

CNTFETs show very high current-carrying capacity which originates from the near-ballistic carrier transport in the SWNT conducting channels. Multiple parallel SWNTs can

be used in CNTFETs to deliver higher current. A recent report from IBM has predicted that sub-10 nm CNTFETs can deliver current density of 2.41 mA/μm which is at least four times more than that of Si-FETs [13].

The on/off ratio measures the ratio between the drain current in the "ON" state and the drain current in the "OFF" state. The on/off ratio of semiconducting CNTs with small diameter is about $10^5 – 10^7$ which satisfies the requirement for logic transistor applications. However, for large-diameter semiconducting tubes and metallic tubes, the on/off ratio is below 10^3 because of their small bandgap. Thus the elimination of metallic pathways in CNTFETs is highly desired.

Subthreshold slope (S) is a measure of how large a gate voltage is required to change the drain current by a factor of ten in switching the transistor on. Subthreshold slope is determined by equation $S=\frac{dV_{gs}}{d\log(I_{ds})}$, where V_{gs} is gate voltage and I_{ds} is drain current [56].

A small subthreshold slope is desired for low-power operation of transistors. The theoretic limit of subthreshold slope is 60 mV/dec at room temperature for a conventional FET [57]. The subthreshold slope can be lowered by using high-k (high dielectric constant) materials as the gate dielectric layers. In addition, optimizing gate structures can improve electrostatic control and therefore lower the subthreshold slope. For example, CNTFETs using top gate structures and ZrO_2 as dielectrics show subthreshold slope of ~70 mV/dec [58]. CNTFETs with HfO_2 dielectrics and dual gate structures can obtain a subthreshold slope of less than 80 mV/dec [59].

Transconductance (g_m) is a critical parameter of FETs. It can be described as $g_m = dI_{ds}/dV_{gs}$, where I_{ds} is drain current and V_{gs} is gate voltage. The transconductance of CNTFETs is determined by the gate capacitance as well as the electron scattering during carrier transport in the channel. With optimal coaxially-gated structure and ballistic conducting channel, the transconductance of CNTFETs can be up to $60\,\mu S$ [58, 60, 61].

The properties of metal-nanotube contact are another key factor of CNTFETs, as it determines the on-state resistance of CNTFETs. The resistance of metal-nanotube contacts depends on several parameters: the work function of metal, the diameter of SWNTs and contact length [62-64]. Recent experiments have shown that the metals with high workfunction, such as Pd, can form p-type transistors with low contact resistance (Ohmic contact) [10]. CNTFETs using low workfunction metal contacts, such as Sc, Y, can be n-type transistors [65, 66]. The contact resistance can also be lowered by using large diameter SWNTs, as the small bandgap in the large diameter tube can reduce the height of Schottky barrier at the contacts [67, 68]. In addition, the contact length is another parameter that affects the contact resistance. Experiments have shown that contact resistance increases dramatically with reduction of contact length [53, 69].

The gate structures of CNTFETs determine the effectiveness of the electrostatic control over the conducting channel. Theoretical calculation indicates that wrap-around gates (Figure 9a)) can offer the optimal electrostatics for CNTFETs [70, 71]. However, the fabrication process of wrap-around gate structure can be very challenging.

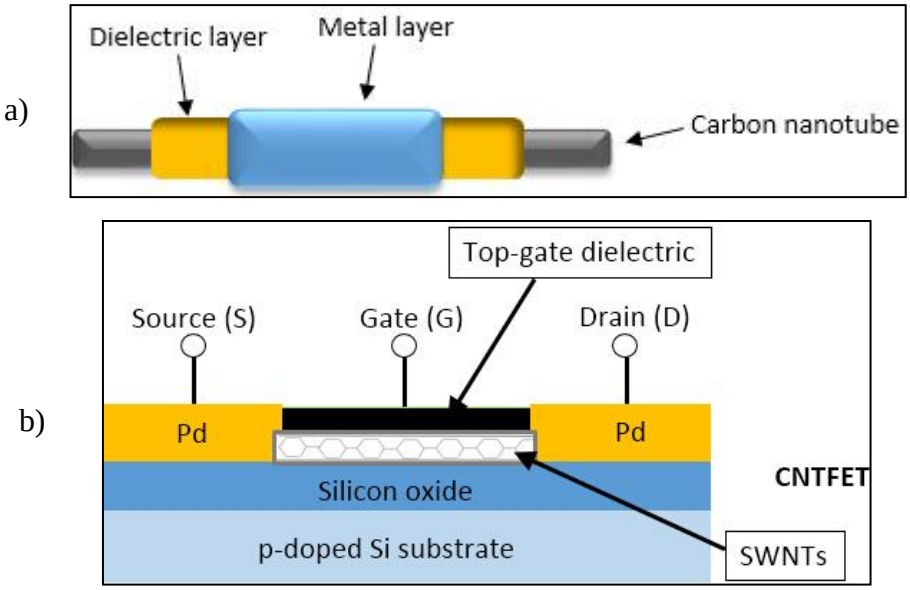

Figure 9: Schematics of wrap-around gate and top-gate CNTFET structures

The first CNTFETs were fabricated with highly doped silicon backgate and silicon oxide dielectric layer [54, 55]. The backgate structure is simple to fabricate, but its electrostatic control is poor. CNTFETs using top-gate (Figure 9b)) or dual gate structures can significantly improve the electrostatics [58].

1.4 SWNT Networks and Their Electrical Properties

SWNT networks are two-dimensional materials comprised of single-walled carbon nanotubes (Figure 10).

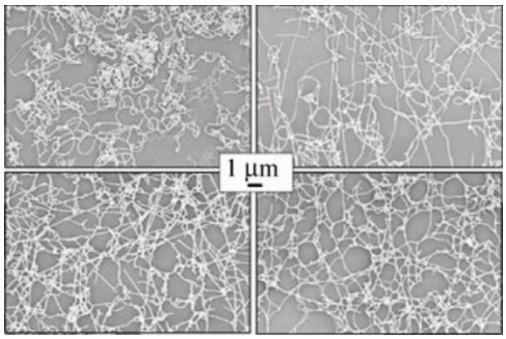

Figure 10: AFM images of some SWNT networks [72].

SWNT networks can be fabricated in various ways and the fabrication methods can strongly affect their electronic properties. A straightforward technique to fabricate SWNT network is via direct solution deposition [73-75]. Nanotubes can be dropcasted on the target substrate (Figure 11a)). The SWNT networks are formed after evaporation of the solvent. SWNT networks can also be fabricated via other solution deposition methods, such as spin coating (Figure 11b)) and Langmuir-Blodgett deposition [76].

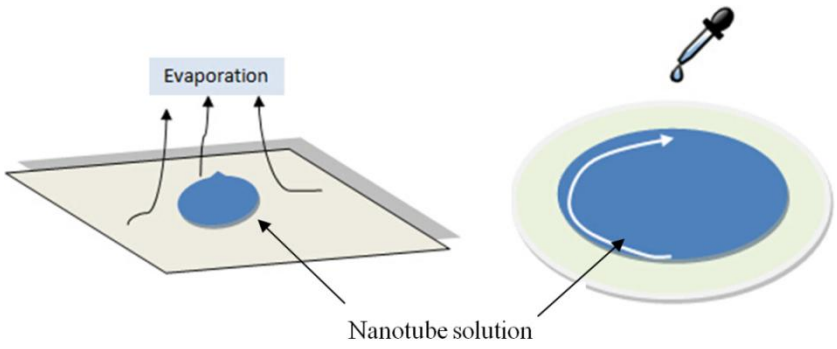

Figure 11: Schematics of SWNT network fabrication process as: a) direct solution deposition; b) spin coating.

The vacuum filtration method (Figure 12) is another kind of solution deposition approach. In this method, SWNTs induced by vacuum are flowed through a porous membrane and

the SWNTs are trapped on the filter [77, 78]. In the following step, the SWNTs covered on membrane are transferred to the desired substrates by dissolving the membrane [78]. By using the filtration method, the density of SWNT networks can be precisely controlled by varying the volume of SWNT solution through the membrane. In addition, it is very simple to obtain a uniform and dense SWNT network film. Therefore this method is widely used for high density SWNT networks for applications such as transparent conductive coatings [78].

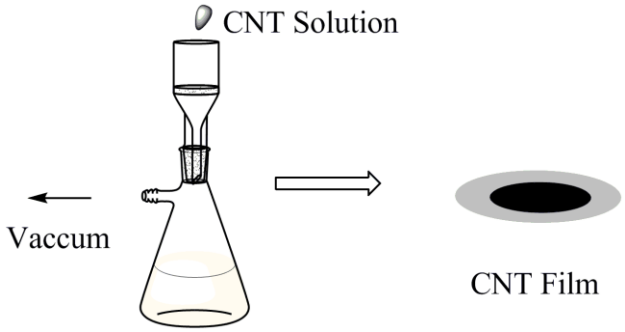

Figure 12: The illustrations of vacuum filtration process [79].

Controlled flocculation (cF) is another method used to fabricate SWNT networks [80, 81]. This approach introduces a SWNT surfactant suspension on the substrate surface with the addition of a solvent, such as methanol (Figure 13). When these two solutions are mixed at the surface of the spinning substrate, the SWNTs are driven out of its stabilized suspension and deposited on the substrate. In the cF method, the density of SWNT networks can be controlled by altering the volume of SWNT suspension. This method is compatible with many substrates without any chemical modification.

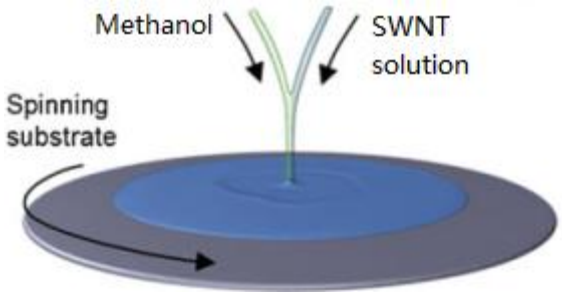

Figure 13: Illustration of the controlled flocculation process [82].

Beyond the solution deposition methods described above, SWNT networks can also be fabricated by direct growth on substrates via chemical vapor deposition (CVD) processes [83-85]. In the CVD process, SWNTs are grown on substrates via high temperature reactions which decompose gas such as CO or hydrocarbons. The metal particles including Fe, Ni, Co, Mo are used as catalysts for CNT growth [83, 86]. The SWNT networks obtained by the CVD process have less bundles, compared to the ones obtained through solution deposition [87].

These methods are simple, cost-effective and compatible with a variety of substrates. However they have some common drawbacks: The SWNT network lacks homogeneity and uniformity; the strong inter-tube interactions cause SWNTs bundling; Surfactants added in the SWNT dispersion can reduce tube bundling and thus improve the uniformity of the SWNT networks, but the surfactants can also lead to adverse effects on the tube electronic properties.

Thin film transistors based on carbon nanotube networks show promising electrical properties. Compared to individual semiconducting SWNT-FETs, the SWNT networks can carry higher current due to the multiple conducting pathways in the networks with

elimination of metallic SWNTs, the transistors based on SWNT networks show current-carrying density of > 40 $\mu A/\mu m$, subthreshold slope of 70 mV/dec and on/off ratio of > 10^5 [88]. The on-state current can be elevated by increasing the tube density in thin film. Current density of more than 100 μA/μm has been realized in SWNT thin film with hundreds of tubes per micrometre [89, 90]. However, SWNT networks contain many tube-tube junctions which cause scattering and lower the carrier mobility [91, 92]. Therefore, SWNT networks with well ordered structures are of importance, because it opens a potential path to control the fabrication of the SWNT networks and make SWNT networks viable for electronics and other applications. Patterned SWNT networks are seen as promising materials for various electronic applications, such as thin film transistors, field-emission displays (FEDs) and chemical sensors [16, 77, 93-95].

1.5 Thesis Summary

In this thesis, a simple and cost-effective method to fabricate patterned SWNT networks is investigated. The detailed procedure of a SWNT network patterning process is discussed in Chapter 2. Background information on colloidal lithography is introduced, and the preparation of a colloidal mask is presented. In the following section, fabrication procedures of the patterned SWNT networks are discussed in detail. In addition colloidal mask removal techniques and device fabrication procedures are detailed.

The characterization of the patterned SWNT networks is presented in Chapter 3. The colloidal masks are inspected by optical microscopy. The morphology of SWNT networks are characterized by atomic force microscopy (AFM) and scanning electron microscopy (SEM) after the removal of the colloidal mask. Electrical measurement shows 2-terminal

and 3-terminal transport characteristics of the patterned SWNT networks and field effect devices. Raman microscopy also provides additional information about the SWNT networks, such as the diameter of SWNTs and structural quality.

Electrical properties of the SWNT networks are discussed in Chapter 4. The electrical transport characteristics of the patterned SWNT network FETs are compared to other FETs. A performance matrix, including parameters such as on/off ratio, transconductance and subthreshold slope is assessed. In addition, the formation mechanism of the patterned SWNT networks is discussed

A conclusion and discussion of future work is contained in Chapter 5.

Some results of this thesis led to a conference paper [96] and a journal manuscript is under preparation [97]

2 FABRICATION OF PATTERNED SINGLE-WALLED CARBON NANOTUBE NETWORKS

In this chapter, we briefly introduce the methodologies of colloidal lithography and its applications in section 2.1. The fabrication process of the patterned single-walled carbon nanotube networks developed in this work based on colloidal lithography is then discussed in detail.

2.1 Introduction to Colloidal Lithography

Periodic nanoscale structures have potential application in bio-electronics, nanoelectronics and nanophotonics. Nanofabrication is a process for fabricating nanoscale functional structures used for manufacturing integrated circuits, biosensors, nanoelectromechanical systems (NEMS) and other applications [98]. Photolithography is the most widely used nanofabrication lithography technique, but it meets difficulties when fabricating sub-wavelength patterns because of its diffraction-limited resolution that make it complex to fabricate nanoscale structures [99, 100]. E-beam lithography as well as scanning probe lithography are well developed to fabricate nanoscale features but low throughput of these two methods has limited their application in industry [100, 101]. Though nano-imprint lithography (NIL) and soft lithography can achieve sub-100 nm features sizes with high throughput, the fabrication of the NIL template can be very challenging [102]. As another alternative option for nanolithography, colloidal sphere lithography using two-dimensional colloidal arrays as masks shows potential to fabricate nanostructures with high resolution and low cost.

Colloidal spheres such as polystyrenes or silica in solution can be self-assembled into a colloidal monolayer which can act as lithographic mask for metal evaporation and etching [100, 103, 104]. As shown in Figure 14a), metal deposition on a colloidal monolayer can reach the substrate through the interstices between hexagonally closed packed colloidal spheres and form an array of nanoscale features with triangle shape. For metal deposition on colloidal double layer (as shown in Figure 14b)), hexagonal arrays of nanoparticles with smaller size can be obtained. Since a colloidal solution is much cheaper than the mask or mold used in other lithography techniques, the cost of colloidal lithography is low Also, the shape and size of particles obtained by colloidal lithography can be modified by changing the size of colloidal spheres [104], deformation of colloidal spheres [105] as well as changing angle between surface of sample and metal source beam [106].

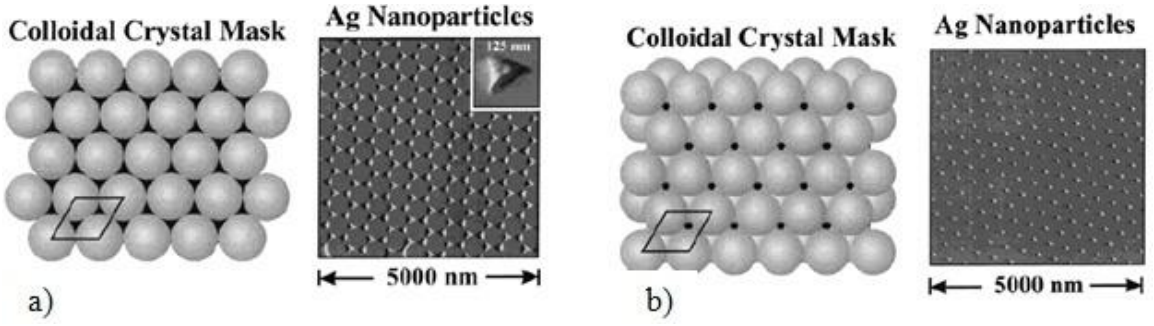

Figure 14: Simplest examples of colloidal lithography. a) Schematic illustration (left picture) and representative AFM image (right picture) for metal deposition on colloidal monolayer; b) Schematic illustration (left picture) and AFM image (right picture) for metal deposition on colloidal double layer [100]

Patterning nanoparticles from solution by colloidal masks is applicable by either dropcasting nanoparticle solution on colloidal monolayer region or immersing colloidal monolayer in nanoparticle solution [106-110]. For this method, patterned ring arrays of nanoparticles are frequently observed. By modifying solution concentration and wettability

of solvent and surface of substrate, two-dimensional nanoparticle mesh and network can be also obtained. Some patterned nanostructures by solution evaporation are shown in Figure 15.

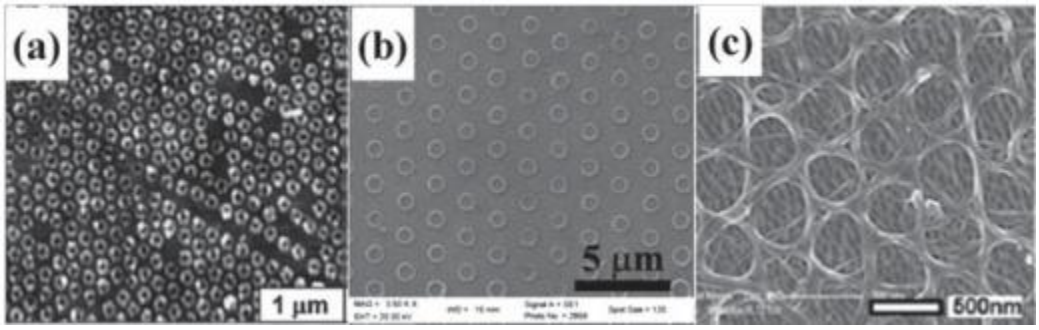

Figure 15: Some examples of patterned nanostructure by solution evaporation via colloidal lithography: (a) Octadecyltrichlorosilane (OTS) nanoring arrays fabricated using vapor deposition through colloidal particle masks; (b) TiO_2 ring arrays synthesized by an annealed template induced sol-soaking strategy; (c) SEM image of CNT networks fabricated by convective assemble of colloidal spheres and micrometer CNTs, and then selectively eliminating the colloidal particles [106].

Inspired by this solution-based colloidal lithography technique, we developed a method to fabricate patterned single-walled carbon nanotube networks on electrode substrates via CNT solution deposition on colloidal monolayers.

2.2 Preparation of Substrate with Patterned Electrodes

In our experiments, heavily-doped p-type silicon wafers (~ 525 nm thick) were used as substrates and coated with a thermally-grown 100 nm thick silicon oxide layer on both sides. On one side of wafer, patterned Ti/Au (1-2 nm/50-100 nm thick) electrodes were fabricated by photolithography. A schematic of the patterned electrode substrates is shown in Figure 16.

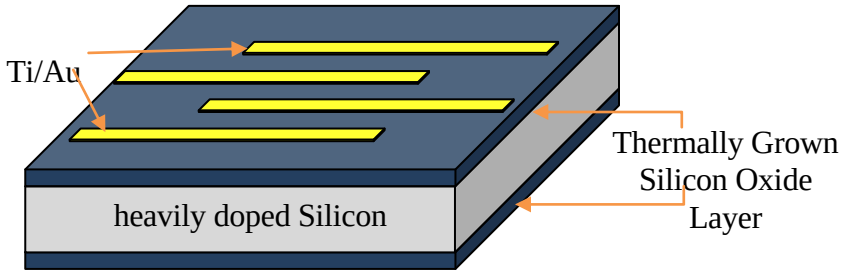

Figure 16: Photo-lithographically patterned electrodes atop oxide-coated, heavily doped silicon substrates.

Two types of patterned electrodes, 4-leg electrodes and interidigitated electrodes were used in our experiment as shown in Figure 17. Before any further use, patterned electrode substrates were all cleansed by bath sonication in acetone to remove residual photoresist from the photolithography process. Thorough rinsing with acetone, isopropyl alcohol (IPA) and deionized (DI) water in turn was followed after sonication. Patterned electrode substrates were finally dried by blowing in nitrogen gas. This cleaning method applies to all substrates used in this thesis.

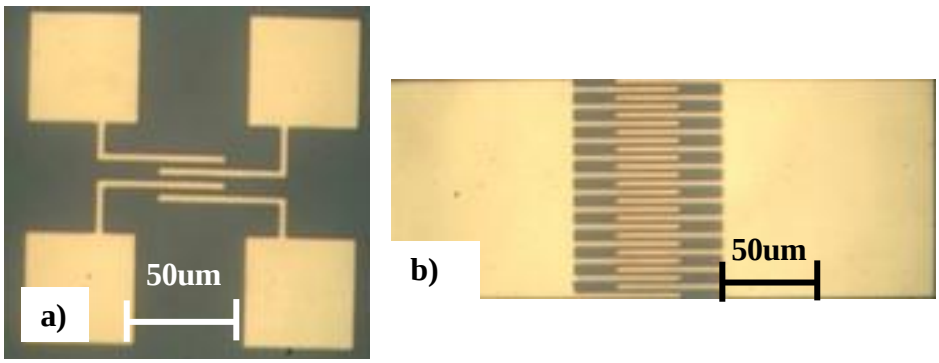

Figure 17: Optical images of patterned electrodes: a) 4-leg electrode pattern; b) 100 µm long interdigitated electrode pattern. Spacing between adjacent electrodes varies from ~ 1 µm to ~ 3 µm.

2.3 Preparation of Colloidal Sphere Solution

Two types of colloidal spheres were used in our experiments. One is polystyrene aqueous suspensions (diameter of polystyrene spheres is 780 nm) purchased from Interfacial Dynamics Corporation and the other one is silica aqueous suspensions (diameter of silica spheres is 800 nm) purchased from Bangs Laboratory. Table 1 gives detailed information of these two stock colloidal solutions.

For patterning masks in colloidal lithography, self-assembled colloidal sphere monolayers with hexagonally close packed ordering is desired. Various ways to form monolayer from solution have been developed, such as drop-casting [111], dip-coating [112] and spin-coating [113]. Among those methods, solution drop-casting which simply drops colloidal solution on substrates in ambient air is the easiest way for colloidal monolayer fabrication since no special equipment or conditions are required. Experimental and theoretical studies found that the quality of colloidal monolayers by drop-casting methods depends on wettability of substrate, concentration of colloid spheres in solution and evaporation rate of solution [114, 115].

Sphere Type	Sphere Size	Solid Weight in Stock Solution	Purchase From	Dispersion
Polystyrene spheres with carboxyl surface groups	780 nm	~ 4 wt%	Interfacial Dynamics Corporation	Aqueous
Silica spheres with natural hydroxyl surface groups	800nm	~ 10 wt%	Bangs Laboratory	Aqueous

Table 1: Product information for stock colloidal sphere aqueous solutions

In our experiments, we applied simple drop-casting for the fabrication of colloidal monolayers on patterned electrode substrates. Polystyrene colloidal spheres with different concentration (from 4 wt % to 0.02 wt %) were tested on 4-leg patterned electrode substrates and results are shown in Figure 18. Colloidal solutions with higher concentration tend to form multilayers of colloidal spheres after evaporation as shown in Figure 18a). With further diluted colloidal sphere solutions, colloidal monolayers were formed on substrates. It was observed that the colloidal spheres assembled on gold rather than the silicon oxide surface. Well-ordered monolayers were also more likely to form on the gold surface. This phenomenon can be explained by the different wettability of gold and silicon oxide [116, 117]. Aqueous colloidal dispersion wets well on a clean gold surface [116] rather than on silicon oxide surface [117].

As shown in Figure 18, the polystyrene colloidal solution with concentration of 0.02 wt% ~ 0.04 wt% can obtain best monolayer formation on patterned 4-leg electrode substrates by drop-casting and drying in ambient air. Silica colloidal monolayer formation from drop-casting method were also tested in a similar way and results showed optimal concentration of silica colloidal solution for monolayer formation is around 0.025 wt%-0.05 wt% for our electrode substrates.

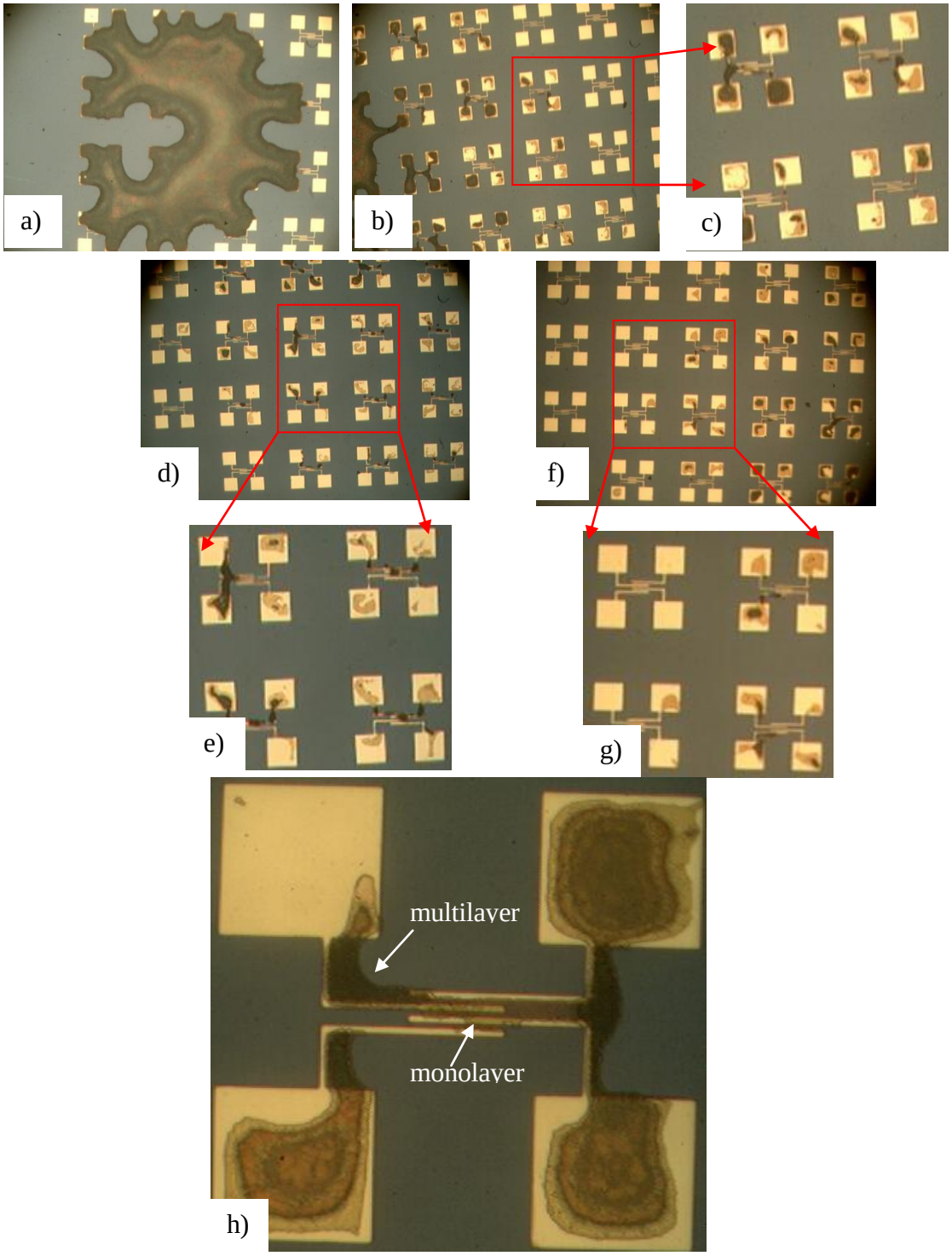

Figure 18: Optical images of colloid deposition after evaporation of polystyrene colloidal solutions with different concentration: a) 4 wt%; b-c) 0.4 wt%; d-e) 0.04 wt%; f-g) 0.02 wt%; h) Illustration of colloidal monolayer and multilayer

2.4 Fabrication Procedure of Patterned Single-Walled Carbon Nanotube Structure

Using colloidal monolayer masks, nanoparticle patterning by solution deposition has been extensively studied [107-110, 118-121]. It was observed that during solution evaporation nanoparticles were attracted to the contact area of colloidal spheres and thus formed patterned structures around the bottom of the spheres. By controlling the colloidal sphere monolayer size or concentration of nanoparticle solution, various patterned structures, such as ordered ring arrays, networks, and meshes can be obtained.

Two types of fabrication methods are generally used for nanoparticle patterning via solution deposition by colloidal lithography. One method is nanoparticle solution deposition on pre-existing colloidal monolayers: Colloidal monolayers are first prepared on a substrate followed by drop-casting of nanoparticle solution. The other method is deposition of a mixed nanoparticle and colloidal solution on substrates: Colloidal spheres nucleate into two-dimensional monolayer during solution evaporation. At the same time, nanoparticles self-assembled around colloidal monolayer and thus form patterned structures. For the latter method, the colloidal solution and nanoparticle solution should be homogenous (in most cases, both solutions are aqueous). In our experiments, both fabrication methods were developed to pattern CNT networks on patterned electrode substrates: CNTs in chloroform and methanol solutions were used for the former method and CNTs in aqueous solution with SDS surfactant was used for the latter method. Detailed fabrication procedures of both two methods are discussed below.

2.4.1 CNT solution deposition on pre-patterned colloidal sphere monolayers

In this set of experiments, both polystyrene and silica colloidal solutions with concentration of 0.02 wt% to 0.05 wt% were used. SWNTs with diameter of 1.2 - 1.5 nm and length of 2 - 5 μm were purchased from Sigma-Aldrich. Chloroform and methanol were used as solvent for CNTs. The concentration of CNTs in chloroform and methanol solution is about 0.3 mg/mL and < 0.1mg/mL, respectively [122, 123]. As shown in Figure 19, colloidal sphere monolayers were first prepared by drop-casting 2.5 μL of colloidal solution on clean patterned electrode substrates and drying in ambient air (Figure 19a) and b)). Next, well-dispersed CNTs in organic solvent were applied on top of the colloidal monolayer regions. During solvent evaporation, CNTs wrapped around at bottom of spheres and formed connections between rings due to capillary force (Figure 19c) and d)). Patterned CNT networks were thus obtained. After solvent evaporation, heat treatment at 95°C was done on all samples to improve adhesion of CNT networks to the substrate. Lastly, the colloidal spheres were removed as shown in Figure 19e) (sphere removal technique is discussed in section 2.5).

In particular, CNTs in chloroform solvent were applied on silica colloidal monolayers and CNTs in methanol solvent were applied on polystyrene colloidal monolayer. Both chloroform and methanol evaporated very quickly and this avoided disturbance of the colloidal monolayer on the surface.

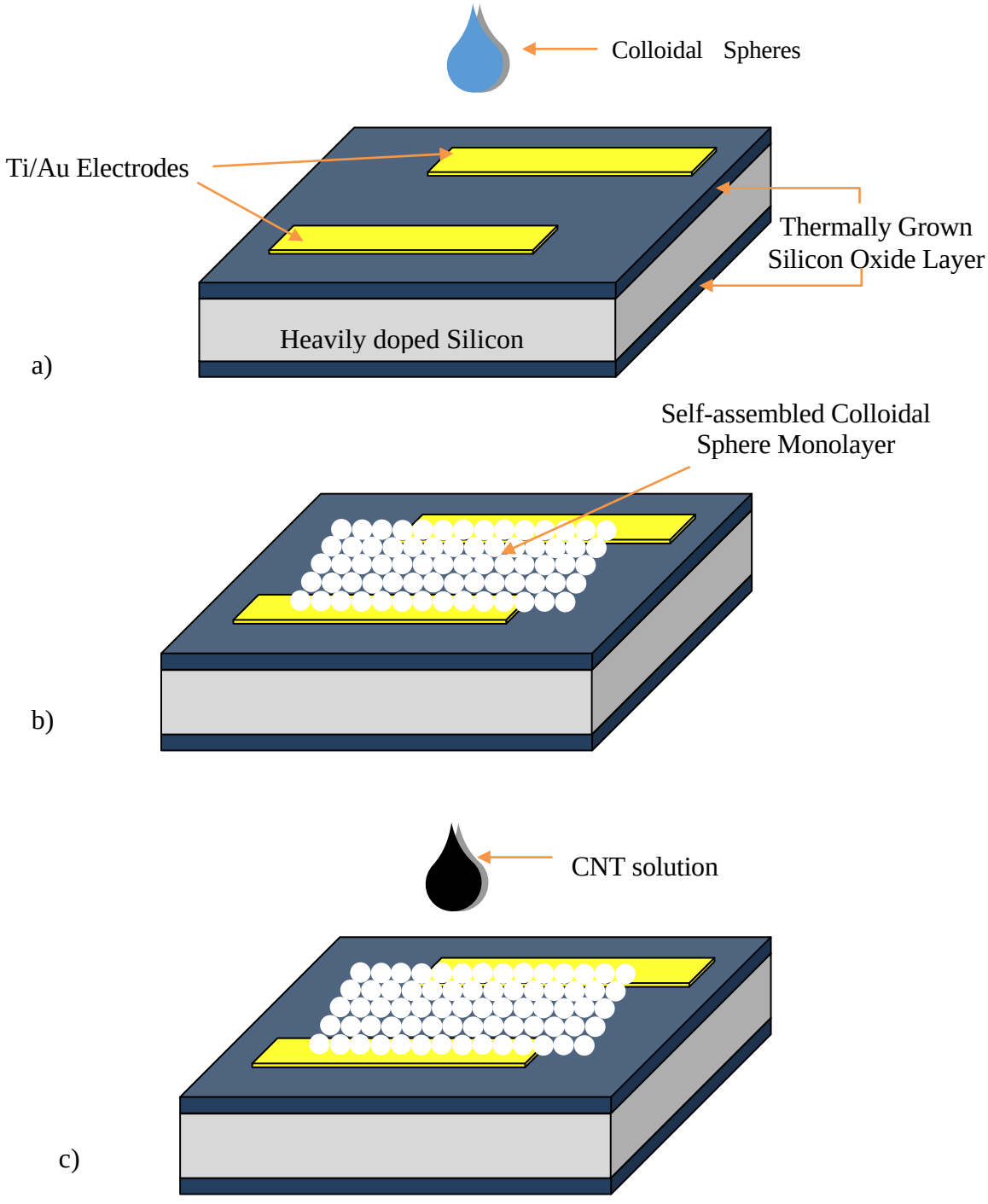
Colloidal Spheres
Ti/Au Electrodes
Thermally Grown
Silicon Oxide Layer
Heavily doped Silicon
a)
Self-assembled Colloidal
Sphere Monolayer
b)
CNT solution
c)

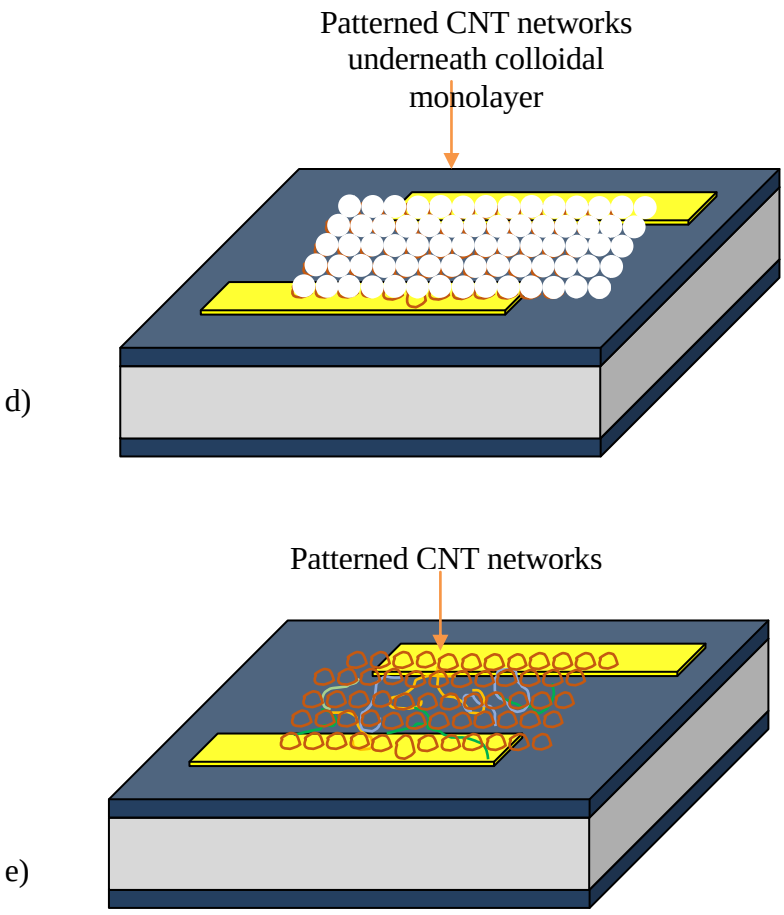

Figure 19: Schematics of fabrication process - solution deposition on pre-patterned colloidal monolayer method: a) Drop-casted colloidal monolayer on clean patterned electrode substrate; b) Colloidal monolayer formed after solution evaporation; c) CNTs in organic solution drop-casted on top of colloidal monolayer region; d) CNT self-assembled at bottom of colloidal monolayer; e) SWNT networks after colloidal spheres removal.

2.4.2 Drop-casting of mixed colloidal sphere and CNT solution on substrates.

In this set of experiments, the Sigma-Aldrich CNTs mentioned in section 2.4.1 were dispersed in distilled water with sodium dodecyl sulfate (SDS) surfactant which

dramatically improved solubility in aqueous solution [124]. The concentration of CNTs was ~ 2 mg/200 mL (0.001 wt%). As shown in Figure 20, CNT aqueous solutions with SDS surfactant were first mixed with polystyrene and silica colloidal solution, respectively. 50 μL 0.04 wt% polystyrene colloidal solution was mixed with 20 μL CNT aqueous dispersion. 25 μL 0.08 wt% silica colloidal solution was mixed with 50 μL CNT aqueous dispersion. Both mixed solutions were sonicated to achieve good dispersion.

2.5 μL of mixed colloid/CNT dispersion were then drop-casted on clean patterned electrode substrates. It was observed that mixed colloidal and CNT solution wetted the patterned electrode substrate better than pure colloidal solution. This is due to the existence of SDS which greatly reduced the surface tension of aqueous solution [125]. Due to improved wettability of aqueous solution, colloidal monolayer was formed over large area, which was very different than that from colloidal solution without SDS surfactant.

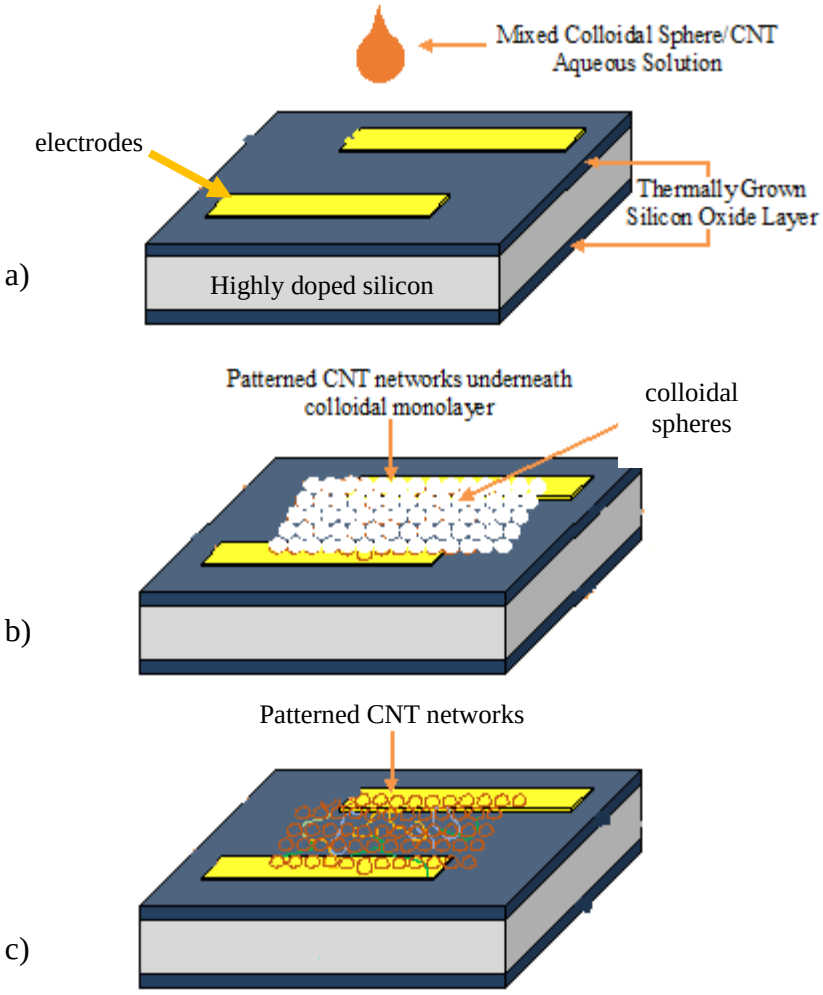

Figure 20: Schematics of fabrication process - mixed colloidal and CNTs aqueous solution drop-casting on substrates: a) mixed colloidal and CNT solution drop-casted on clean patterned electrode substrates; b) Colloidal self-assembled monolayer and patterned CNT networks self-assembled at bottom of colloidal monolayer; c) SWNT networks after colloidal sphere removal.

2.5 Sphere Removal Techniques

In this section three sphere removal techniques are described:

1. Taping

2. Light Sonication in ethanol (typical condition is the lowest power level on VWR 75D bath sonicator for 1 - 10 seconds)

3. Immersing in dichloromethane (DCM) solution

1. A piece of scotch tape was put on top of the colloidal monolayer region of the sample with a little bit pressure. Then tape was peeled off to remove the colloidal spheres. With gentle pressure, the tape was able to remove the colloidal spheres layer by layer. After each taping, the sample was inspected under an optical microscope to check if the colloidal sphere at desired regions were removed or not. Depending on the samples, multiple taping could be done to remove the colloidal spheres.
2. Another option for sphere removal is to sonicate the sample in ethanol. A light sonication in VWR75D sonicator with lowest power level was used. It was observed under the microscope that both colloidal spheres and carbon nanotube were all removed after sonication. Thus even the lightest sonication was too strong to effectively remove the spheres and leave SWNTs.
3. Since polystyrene can be dissolved in dichloromethane (DCM) solution, the samples with polystyrene colloidal spheres were immersed into DCM to remove the polystyrene colloidal spheres. Though polystyrene spheres were removed from the electrode surface, in this case, we found many residues were left on the surface of samples. The residue

caused problems for surface imaging of carbon nanotube networks. Thus DCM dissolution was not deemed a good method for our application.

It was found that taping is the best available method we had to remove the spheres, since no residue from tape was left on the sample.

2.6 Fabrication Process for CNTFET devices

To characterize the field effect behavior of patterned CNT networks, a back-gate contact was fabricated on the substrates. Heavily doped silicon was used as the back-gate contact because of its intrinsic low resistance. As shown in Figure 21, the backside of the substrate was polished using sandpaper to remove the silicon oxide layer and subsequently cleansed by acetone and IPA in turn using Kimwipe paper to remove residues from the sanding process. Silver paint (SPI Supplies) was then brushed on the backside of the substrate and heated in a mechanical oven at 80°C for 60 minutes. A thin layer of indium for the probe gate contact was put underneath substrates and followed by heat treatment at 170°C for 5 minutes to obtain good adhesion between indium paint and substrates. Since both silver paint and indium have low resistance, back-gates with high conductivity were achieved. One type of indium alloy (49% Bi, 21% In, 18% Pb, 12% Sn) with low melting temperature of 58°C was also used to replace indium when low temperature heat treatment was needed (for instance, samples with polystyrene which has glass transition temperature ~ 100°C).

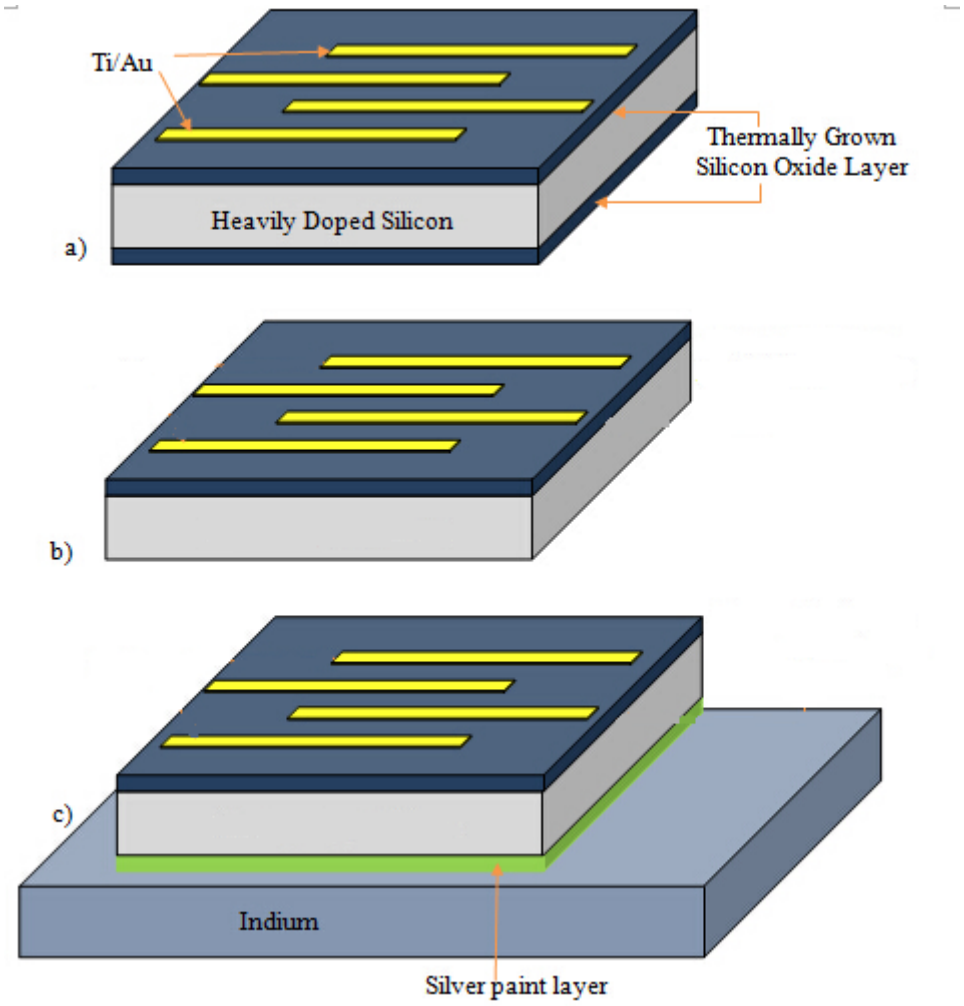

Figure 21: Schematics of back-gate fabrication process: a) Original patterned electrode substrates; b) Silicon oxide layer removed by sanding; c) Silver paint and indium layer was applied at bottom of substrates.

3 CHARACTERIZATION OF PATTERNED SINGLE-WALLED CNTFETS

In this chapter, the morphology of the patterned SWNT networks is characterized and their electrical properties are measured. Since the colloidal monolayer is of importance in the SWNT network patterning process, the formation of self-assembled colloidal monolayer is also examined.

Two different patterned SWNT networks fabrication methods are developed in Chapter 2. In one method, carbon nanotube aqueous solution is dropcasted on the colloidal monolayer on the substrates. In the other method, the colloid and carbon nanotube mixed aqueous solution are dropcasted on the substrates. In our work, two different colloidal spheres, silica and polystyrene are used as colloidal materials. Therefore, there are four independent experimental set-ups, as shown in Table 2. Multiple samples were prepared and characterized for each set-up.

1	Silica nanosphere aqueous solution dropcasted on patterned electrodes, carbon nanotube solution dropcasted on colloidal monolayer
2	Polysterene nanosphere aqueous solution dropcasted on patterned electrodes, carbon nanotube solution dropcasted on colloidal monolayer
3	Mixed silica nanosphere/carbon nanotubes solution dropcasted on patterned electrodes
4	Mixed solution of polystyrene nanosphere and carbon nanotubes dropcasted on patterend electrodes

Table 2: List of four methods proposed to fabricate patterned single walled carbon nanotubes

3.1 Optical Microscopy

The formation of colloidal monolayer was analyzed by optical microscopy. After droplets of colloidal solution on the substrates were completely evaporated, optical images of silica colloidal assemblies were taken by an Olympus optical microscope. As shown in Figure 22, the colloids formed thick multilayers in the center of the colloidal droplets. Colloidal monolayer was mostly observed at the edge of the droplets. It was found that colloids are mostly deposited on the gold surface rather than the silicon oxide surface. Such an interesting drying pattern can be explained by the difference of hydrophobicity of the gold surface and silicon oxide surface [126, 127].

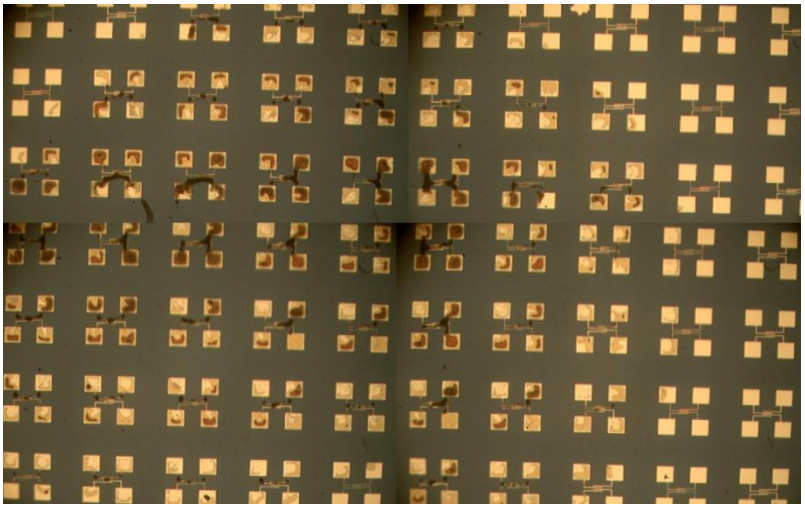

Figure 22: Optical images of the silica colloidal multilayer and monolayer on the substrates.

After the colloidal aqueous solution was dropcasted on the substrates, it spread anisotropically on the substrate surface due to the surface inhomogeneity. The gold surface is more hydrophilic than the silicon oxide surface. Therefore, the droplet has a smaller contact angle on the gold surface than that on the silicon oxide surface. When the solution

is evaporating, the pinning effect occurs at the liquid/air/solid interface, and the colloids start to stack multiple layers. The droplet will slowly move toward gold surface because of imbalance of the surface tension at the droplet on the heterogeneous surface [128, 129]. After the solution was completely evaporated, the colloidal sphere layers were mostly formed on gold surface.

In the other experimental set-up, the colloid and SWNT mixed aqueous solution were dropcasted on the substrates. In this case, a ring-like colloidal pattern was formed on the substrates, as shown in Figure 23. The colloidal multilayer ring formed at perimeter of the ring and the colloidal monolayer formed inside the ring.

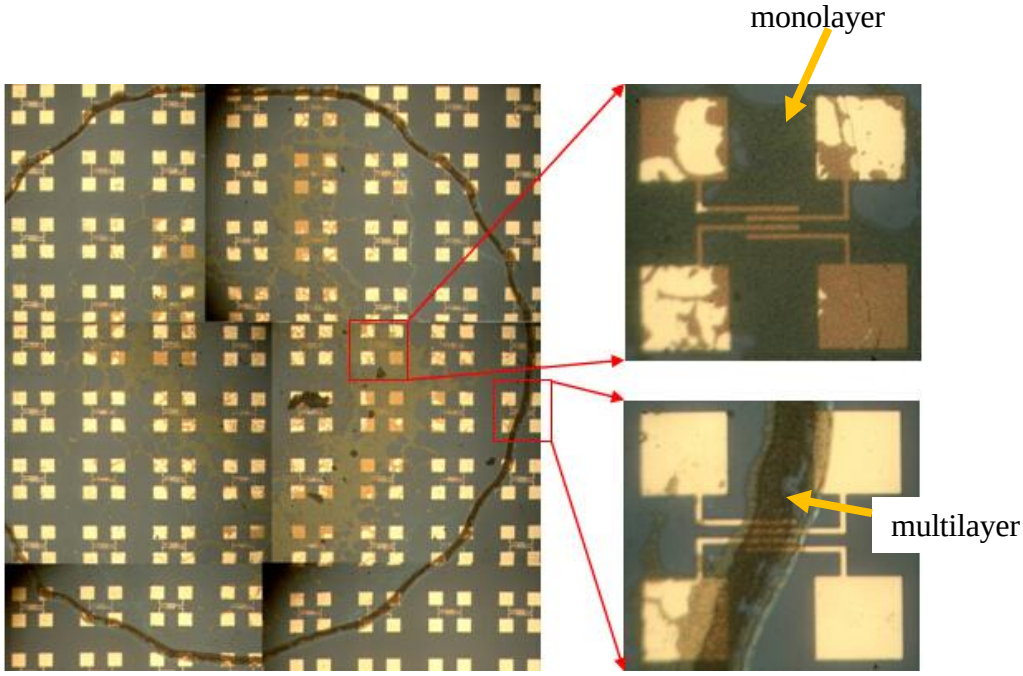

Figure 23: Optical images of the colloidal assemblies formed by depositing mixed carbon nanotube and polystyrene sphere aqueous solution with SDS surfactant.

The formation of the ring-shaped colloidal patterns on the substrates can be explained by contact line pinning of the colloids [130]. The contact pinning effect is caused by capillary forces due to surrounding liquids and by nanosphere-substrate interaction [131, 132].

Because of the contact pinning effect, colloidal spheres were accumulated at the edge of the droplet.

Inside the colloidal ring, the substrates were partially covered by colloidal monolayers. The formation of colloidal monolayers includes to two consecutive steps during the evaporation of solvent: nucleation and crystallization [133]. At the initial stage of solution evaporation, the colloidal spheres are free to move as Brownian motion in the droplet. With further evaporation of the solution, colloidal spheres in the solution became denser and the droplet of colloidal solution becomes thinner. When the height of the colloidal solution became smaller than the diameter of the colloidal particles, the colloidal spheres protrude from the water layer. At this point, the capillary forces induced at the liquid-gas interface became the dominant forces [134]. The colloidal spheres which protruded from the solution are pushed together to form a nucleus by the capillary forces. Once the nucleus is formed, the rest of the colloidal particles are pushed by a convective water flux toward the nucleus and form hexagonal ordered monolayers [135].

In Figure 24, enlarged images of colloidal monolayer areas show that the colloids are orderly arranged over tens of square micron. The left image of Figure 24 illustrates colloidal monolayer with dot and line defects on gold surface. The right image of Figure 24 shows the monolayer colloidal monolayer overlapping both silicon oxide and gold surface. In addition, the transition between the monolayer and the multilayer can be seen. The monolayer regions that cover both electrodes and silicon oxide area are of our primary interest. There are two reasons for this. First, the monolayer formed on the substrates is useful for the carbon nanotube patterning. Carbon nanotube patterned under double or

multiple colloidal layers was low. Second, the patterned carbon nanotube networks formed in this area can be readily used for the measurement of electronic properties

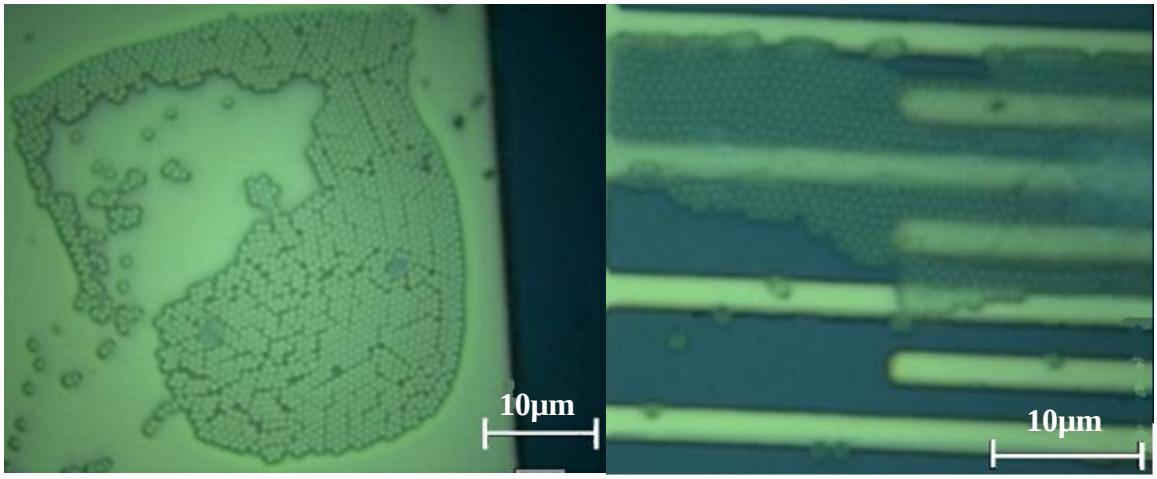

Figure 24: Optical images of colloidal monolayer on the gold surface and on the silicon oxide surface.

3.2 Atomic Force Microscopy

The morphology of the patterned SWNT networks was characterized by an atomic force microscope (MultiView 1000 from Nanonics Imaging Ltd.) with pulled fiber tips after the removal of the colloidal mask by taping.

It was observed that the SWNTs were patterned in ordered structures under the colloidal monolayer. As shown in Figure 25, the patterned SWNT networks formed a ring hexagonal ring array with some SWNTs connected between the rings. This kind of the patterned network was observed in the sample fabricated by drop-casting carbon nanotube solution on the pre-patterned silica microsphere monolayer. It is suspected that the SWNT networks comprised of small SWNT bundles as the height of the patterned SWNT networks is about 4-10 nm (Figure 25b). The diameter of the rings is approximately 300 nm. The spacing

between the rings is about 800 nm which is close to the size of a single colloidal sphere. The nanotubes which connected the rings had an average diameter of 3-5 nm.

Another type of patterned SWNT network is shown in Figure 26. This sample was fabricated by drop-casting mixed carbon nanotube and silica microshpere aqueous solution on the substrates. A ring-like mesh structure was observed. It is suspected that the carbon nanotube mesh structure comprised a mixture of carbon nanotubes and residues. The irregularity of the mesh patterns might be caused by disorder of the colloidal mask.

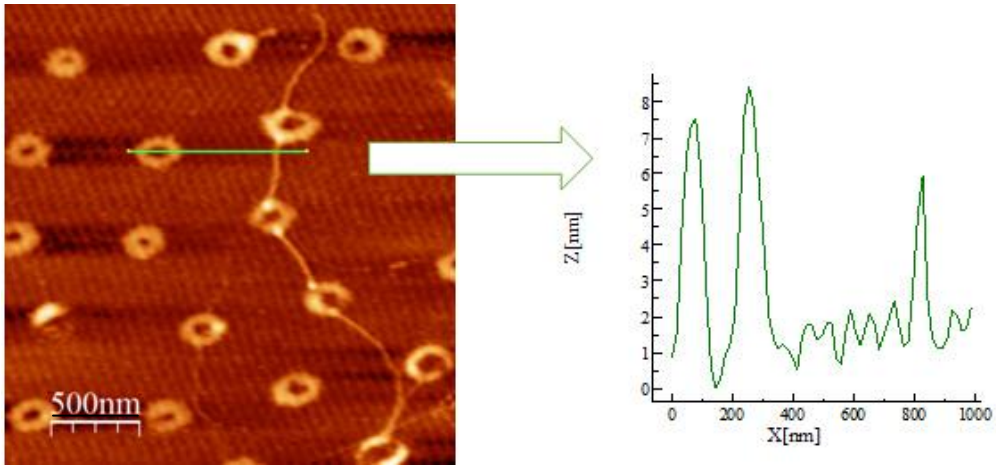

Figure 25: a) AFM image of the patterned carbon nanotube networks (This sample was fabricated by drop-casting chloroform-SWNT solution on the pre-patterned silica microsphere monolayer. Heat treatment was done at 200 °C for 200 minutes. AFM was done after removing colloidal spheres by taping). b) Cross-section profile of green line in left image.

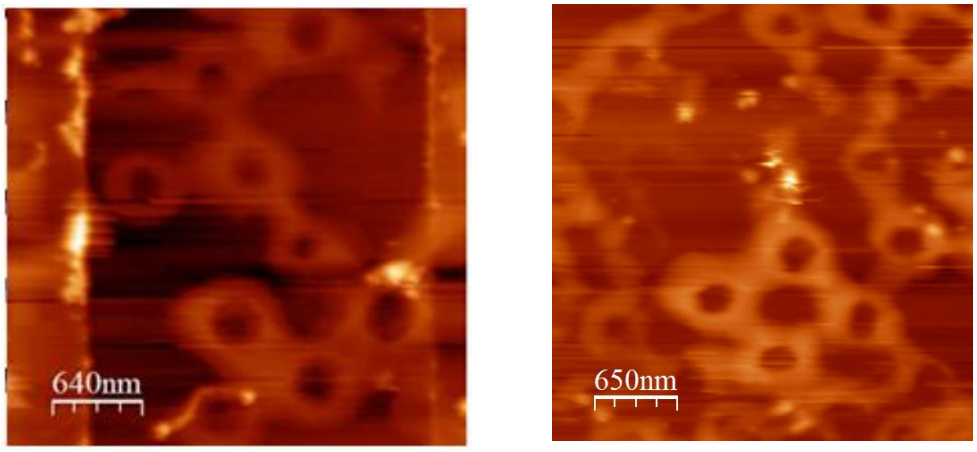

Figure 26: AFM images of patterned carbon nanotube networks near gold electrodes (This sample was fabricated by drop-casting mixed carbon nanotube and silica microsphere aqueous solution on the substrates. SDS (sodium dodecyl sulfate) surfactant was used to improve the dispersion of the SWNTs in aqueous solution. Heat treatment at 95 °C for 10 minutes was done.

Other than the patterned SWNT networks described above, Figure 27 the residues were patterned as an ordered array of rings and solid circles. Their diameter varies from 400 nm to 600 nm and the height is over 10 nm.

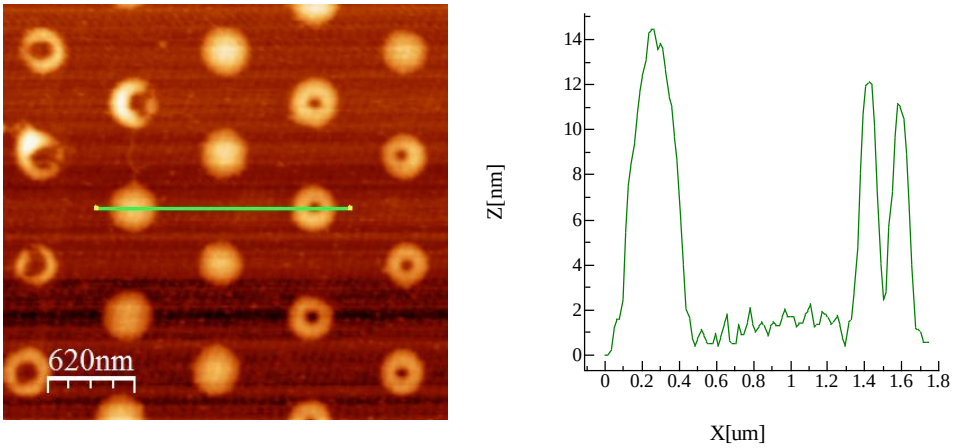

Figure 27: AFM images of patterned residues; solid circles and rings.

3.3 Scanning Electron Microscopy

The morphology of the patterned SWNT networks was also characterized by scanning electron microscopy (SEM). The sample was fabricated by the following procedure: Firstly polystyrene colloidal solution was mixed with mixed with SWNT-SDS aqueous solution; then the mixed solution was dropcasted on the substrates. SEM images were taken after removal of colloidal spheres.

Figure 28 shows a sample that was the patterned SWNT networks on both silicon oxide and gold surface. Some SWNT rings are connected by SWNTs to form networks.

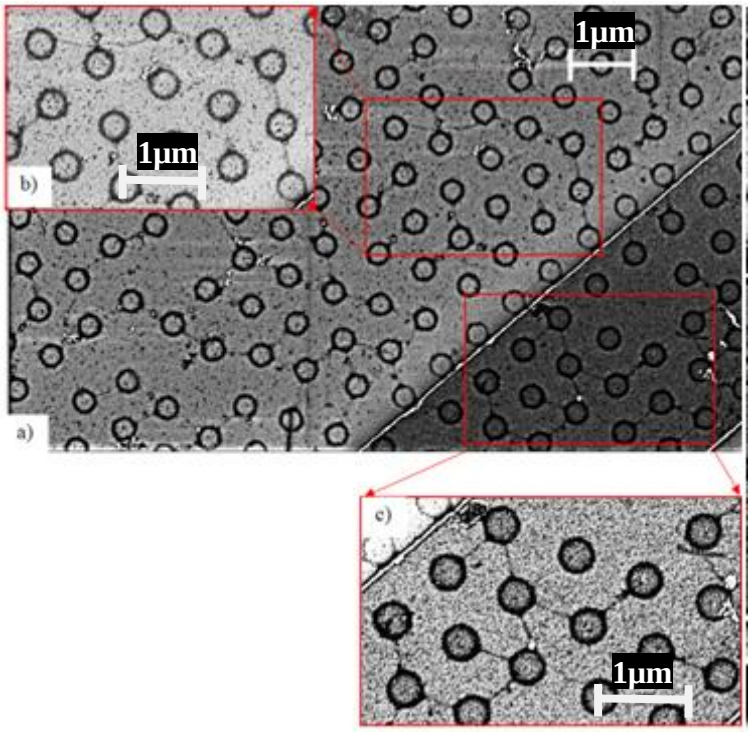

Figure 28: a) SEM images of patterned SWNT networks; b) Close-up image of the patterned SWNT networks on silicon oxide; c) Close-up image of the patterned SWNT networks on gold surface (The contrast and brightness of SEM images were adjusted.

In Figure 29, two patterned networks (in the red squares) between electrodes are shown.

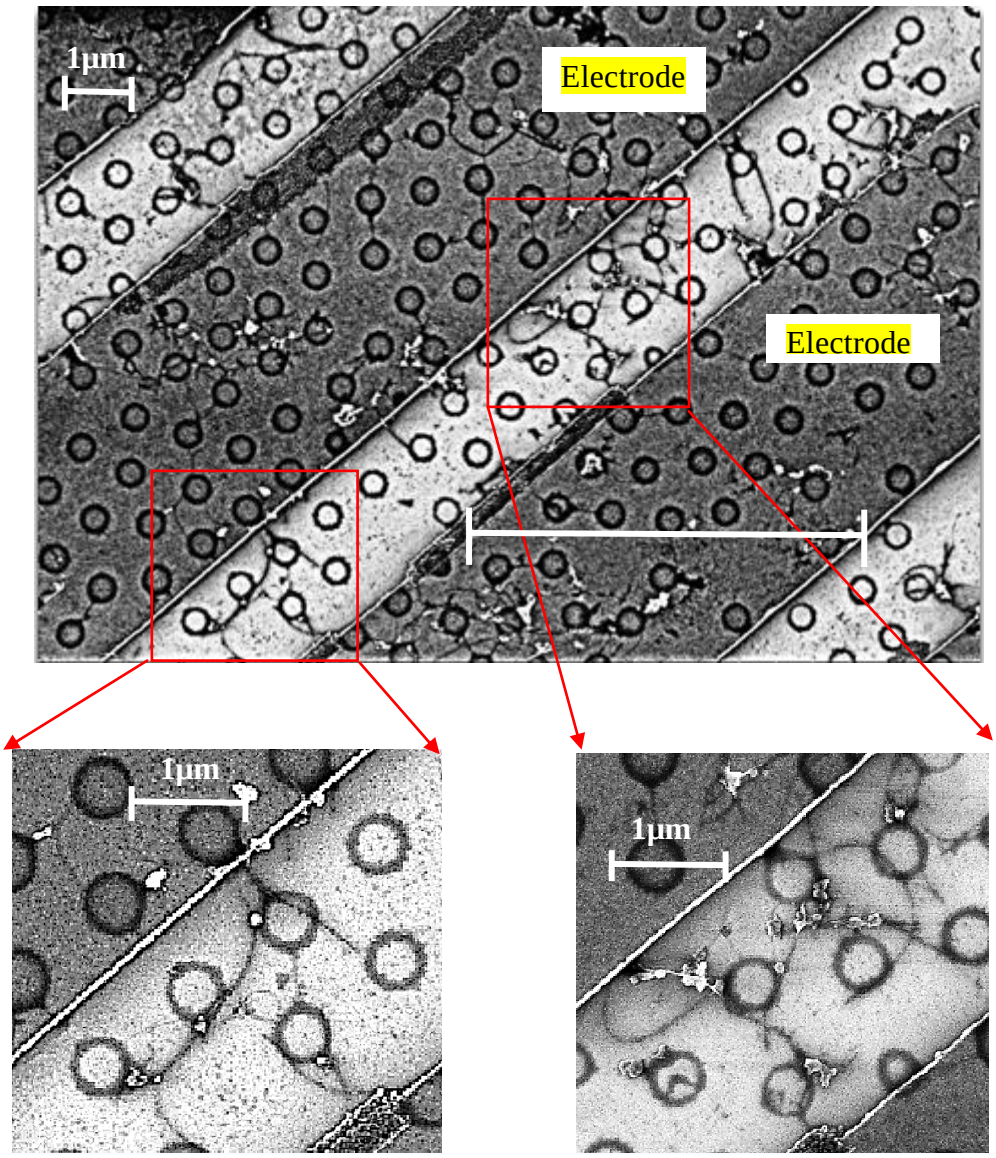

Figure 29: SEM images of patterned SWNT networks between electrodes.

3.4 Electrical Characterization

In this section, the characteristics of electronic transport in the SWNT networks measured using a Keithley 4200 semiconducting characterization system and Janis 4-probe station are presented. The experimental set-up of the electrical measurement is shown in Figure 30. Two tungsten probe tips were connected to drain and source electrodes, respectively. A third probe was connected to the gate electrode. In this work, heavily doped silicon was used as the back-gate contact. The thickness (d_t) of the SiO_2 dielectric layer was 100 nm. The drain voltage was initially swept from -0.5 V to +0.5 V without applying gate bias. The relatively low drain bias was applied to avoid damaging the patterned SWNT networks.

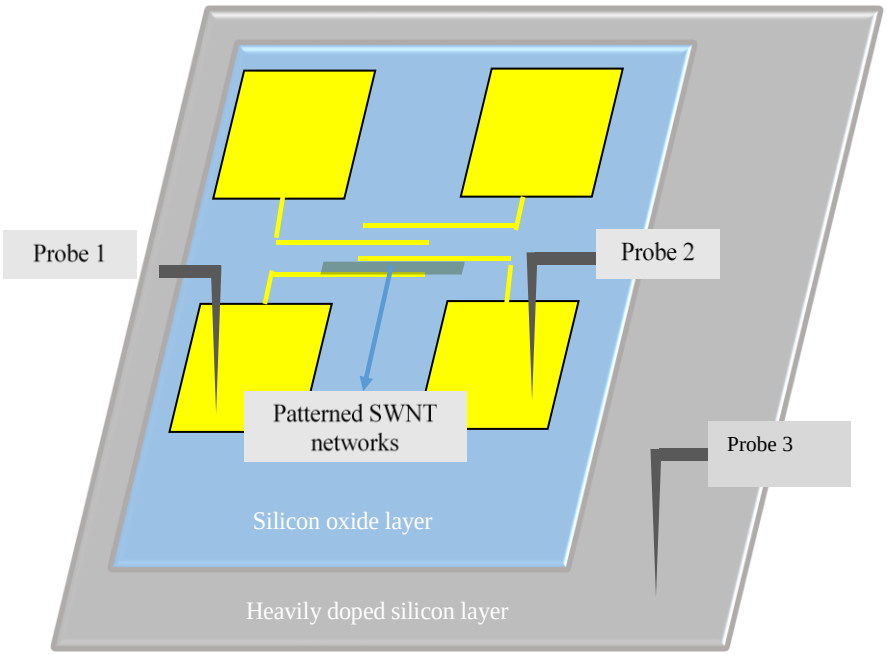

Figure 30: The set-up of electrical measurement of patterned SWNT networks

Depending on the morphology of the SWNT networks, the samples measured were categorized into three groups (Figure 31):

1. Random SWNT networks

2. Partially patterned SWNT networks

3. Fully patterned SWNT networks

The random SWNT networks can be found on the substrate without any coverage of the colloidal monolayer. The partially patterned SWNT networks can be found on areas partially covered by colloidal monolayer. The fully patterned SWNT networks can be found on areas fully covered by colloidal monolayer.

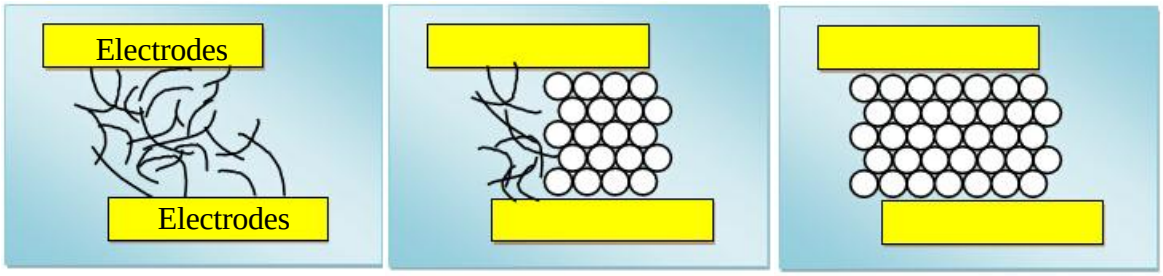

Random SWNT network **(Samples A and B)**

Partially patterned network **(Samples C and D)**

Fully patterned network **(Sample E)**

Figure 31: Schematics of random SWNT networks, partially patterned SWNT networks and fully patterned SWNT networks between electrodes.

3.4.1 Random SWNT networks

The results of two-terminal current-voltage characteristics are shown in Figure 32. The three devices are from sample A in which random SWNT networks were fabricated by dropcasting 5 µL of methanol-SWNT solution on the substrates. The sample was subsequently heated on a hotplate at 170 °C for 200 minutes prior to electrical measurement.

The resistance of the random SWNT networks in sample A is between 3-10 MΩ. The results of three-terminal measurement showed no field effect behaviour in any devices, which indicates that metallic pathways dominated these random SWNT network devices.

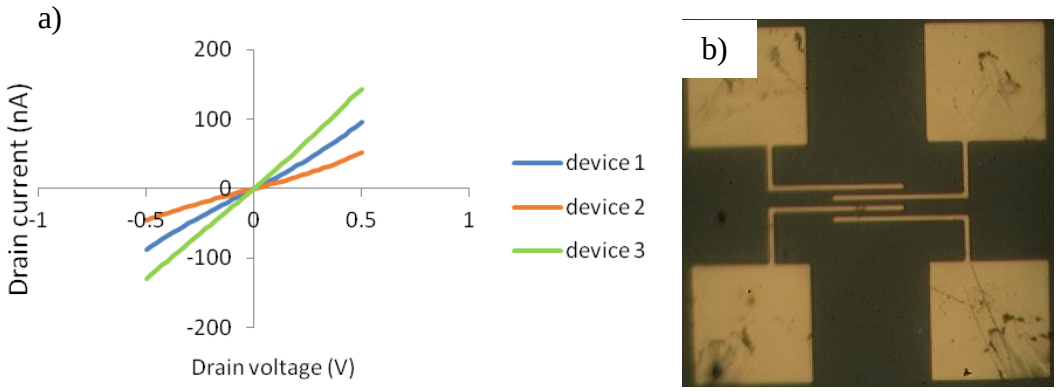

Figure 32: a) Typical two-terminal I-V characteristics of random SWNT networks (Sample A); b) Optical image of device 1.

Figure 33 shows I-V data for another random SWNT network sample (Sample B), which was fabricated by dropcasting chloroform-SWNT solution on the substrate, followed by heat treatment was done at 200 °C for 200 minutes.

I-V characteristics of the random SWNT networks in sample B varied from device to devices. Some devices (for instance, device 1 and 3) showed resistance of hundreds of MΩ. However, the resistance of device 2 is less than 1 MΩ.

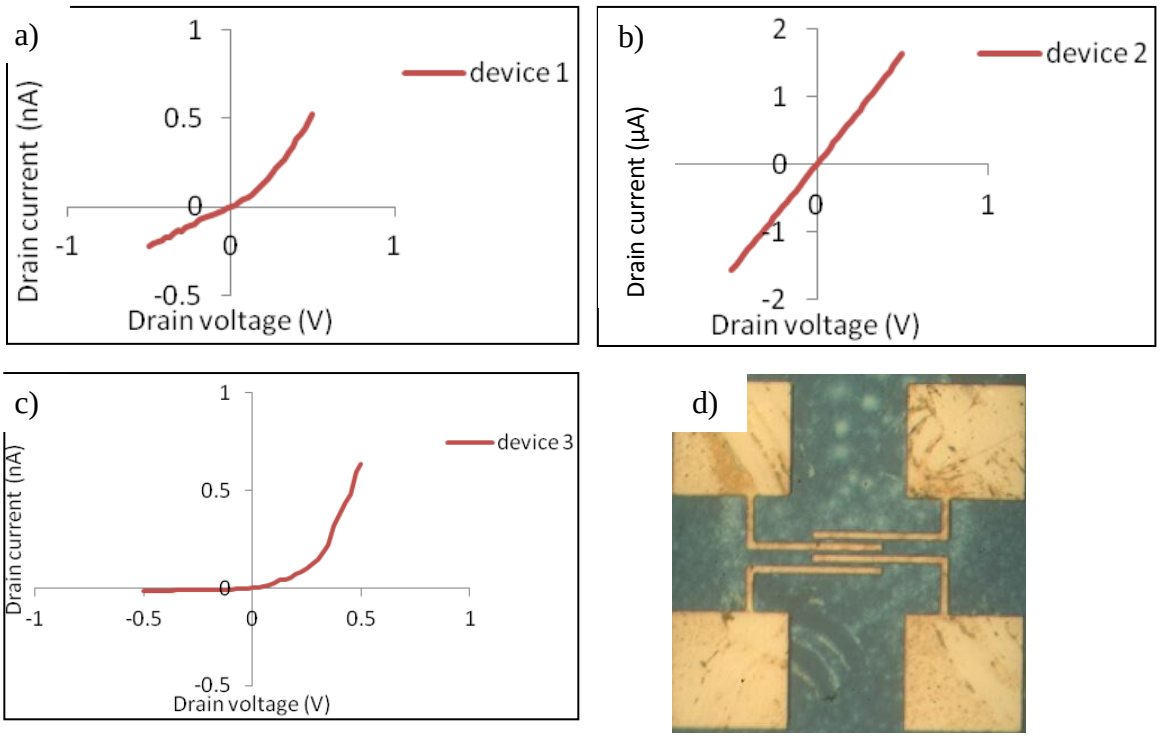

Figure 33: a-c) typical two-terminal I-V characteristics of the random SWNT networks in sample B; d) Optical image of device 3.

Three-terminal measurement showed that the conductance of some devices (for instance, device 1 and 3) can be modulated by gate bias (Figure 34). The nonlinearity of I-V curves may be due to Schottky metal-SWNT contacts. The on/off ratio of both devices is above 100.

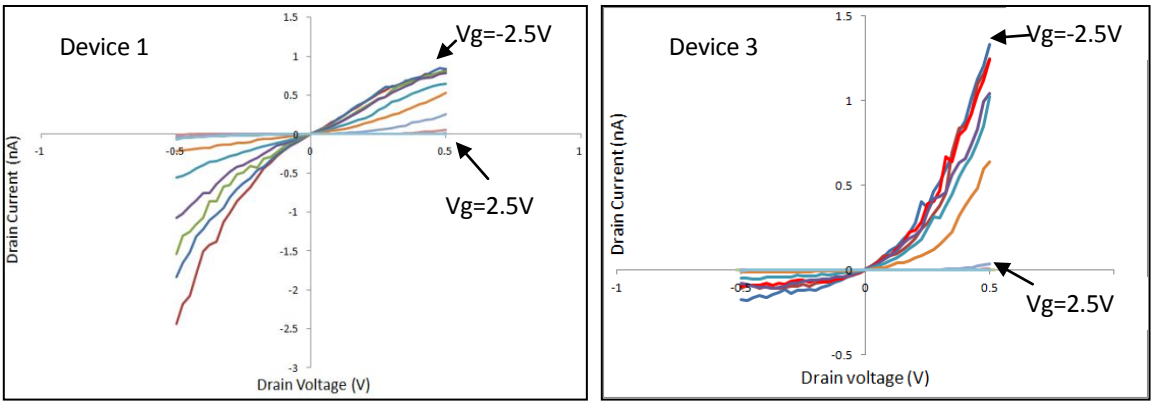

Figure 34: Output characteristics of the random SWNT networks from sample B for different gate voltages.

3.4.2 Partially patterned SWNT networks

The results of two-terminal current-voltage characteristics of the partially patterned networks are shown in Figure 35. Sample C and sample D were fabricated by the following procedure: 2.5 µL of silica colloidal sphere solution was dropcasted on this sample. Subsequently 5 µL of chloroform-CNT solution was dropcasted on the substrate. Heat treatment was done at 200 °C for 200 minutes before electrical measurement.

The resistance of the partially patterned SWNT networks in sample C was about 3-10 MΩ, while in sample D it was about 20-50 kΩ. The results of three-terminal measurement showed no field effect behavior in any devices. This likely indicates that metallic pathways dominated electronic transport in the partially patterned SWNT network devices.

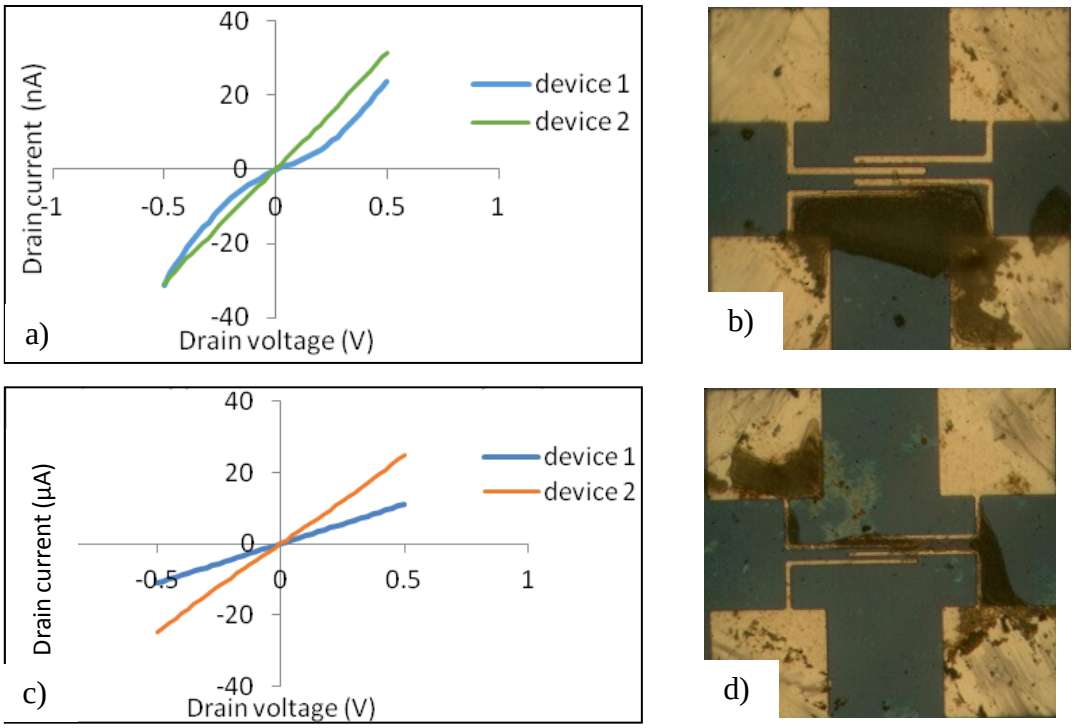

Figure 35: a) Typical two-terminal I-V characteristics of the partially patterned SWNT networks in sample C; b) Optical image of device 1 in sample C; c) Two-terminal I-V characteristics of the partially patterned networks in sample D; d) Optical image of device 1 in sample D.

3.4.3 Fully patterned SWNT networks

The results of two-terminal current-voltage characteristics are shown in Figure 36. Sample E was fabricated by following procedure: 2.5 µL silica colloidal sphere solution was dropcasted on the substrate with prepatterned gold electrodes. After drying of the colloidal solution, 5 µL of chloroform-CNT solution was deposited on top of the colloids. Heat treatment at 200 °C for 200 minutes was done after the evaporation of the solution. The back-gate was fabricated after heat treatment.

The patterned networks have resistance of tens of MΩ, as shown in Table 3. It is assumed that the high resistance is because of the high contact resistance and/or low conducting paths in the SWNT networks.

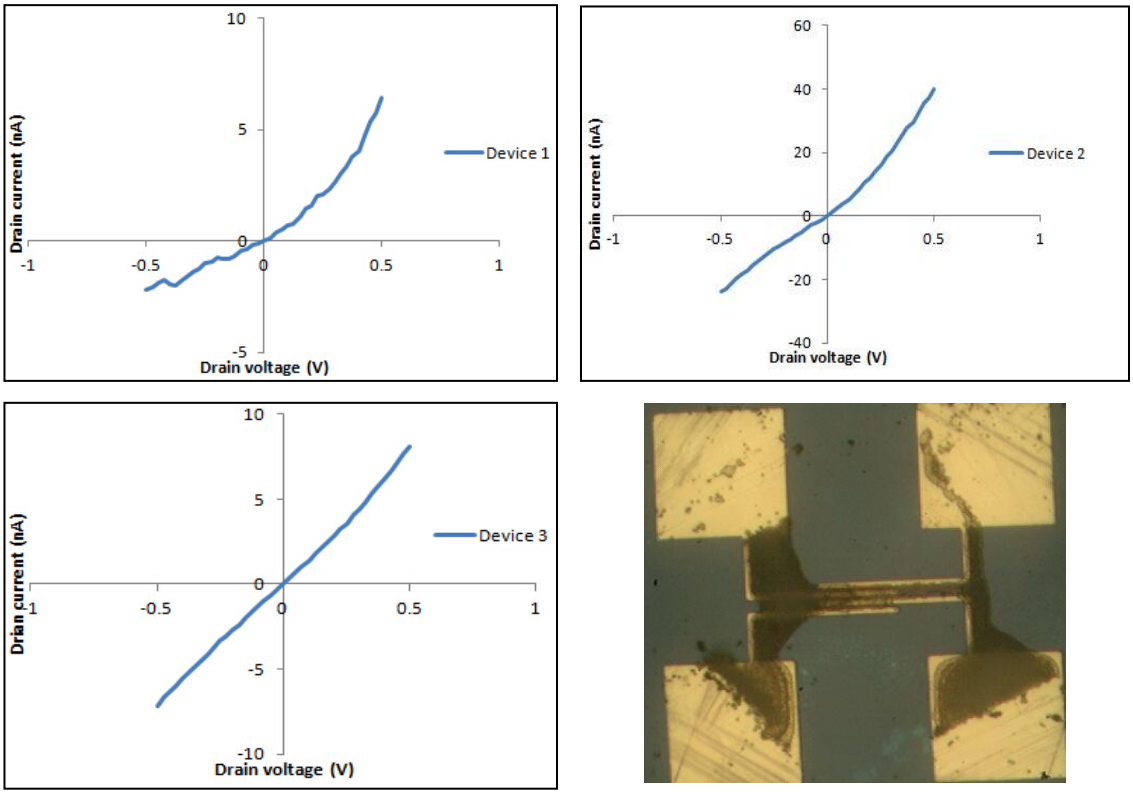

Figure 36: Typical two-terminal I-V characteristics of fully patterned SWNT networks (Sample E).

	Conductance (nS)	Resistance (MΩ)
Device 1	5.07	197
Device 2	43.9	22.8
Device 3	13.5	74.3

Table 3: Zero bias conductance and resistance of fully patterned SWNT networks (derived from Figure 36)

In addition, the field effect characteristics of the patterned SWNT networks were measured. The transfer characteristics and output characteristics of the patterned SWNT networks are shown in Figure 37. The gate voltage was varied from -2.5 V to 2.5 V with steps of 0.5 V.

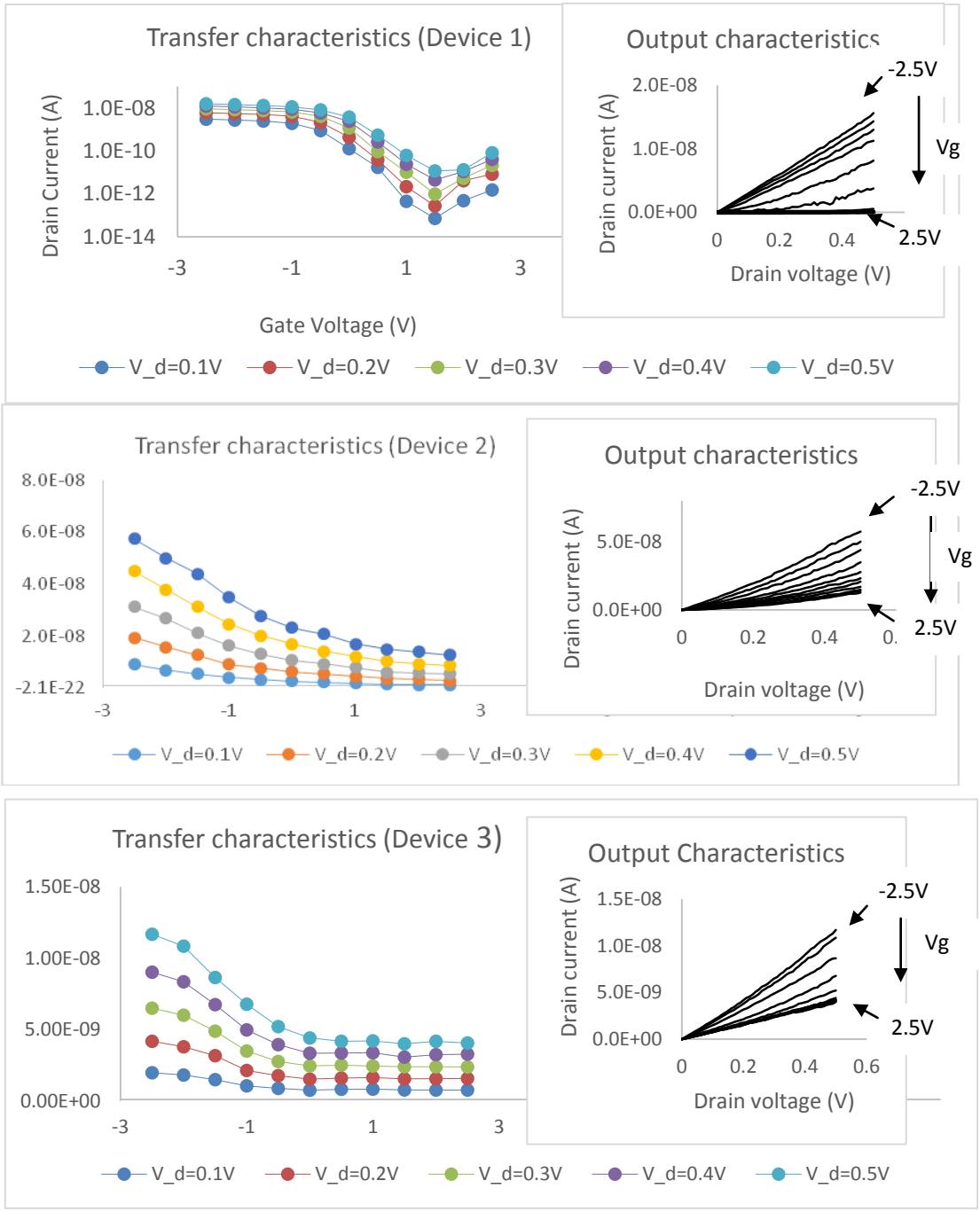

Figure 37: Transfer and output characteristics of the fully patterned SWNT networks (Sample E)

The patterned SWNT networks behave like p-type FETs. The drain current can be lowered with the increase of gate voltage. One exception is device 1, the drain current of which reached a minimum at Vg = 1.5 V and then increased for larger gate bias. Such an ambipolar behavior may be due to the presence of large-diameter, narrow band-gap semiconducting tubes in the conducting path and has been previously observed in field-effect measurements on individual SWNTs [136, 137].

Electrical measurement was also done on the fully patterned devices in sample E after removal of the colloidal spheres. The conductance of the fully patterned SWNT networks was significantly reduced after sphere removal. In many devices, their conductance reduced to zero after removal of the colloidal spheres. This observation indicates that some SWNTs in the networks could be removed during the sphere removal process (by taping).

For the samples fabricated by drop-casting mixed carbon nanotube and silica/polystyrene microsphere aqueous solution on the substrates, their electrical conductance is not available due to lack of experimental data.

3.5 Raman Microscopy

Raman spectroscopy is a spectroscopic tool based on inelastic phonon scattering of monochromatic light. A laser is typically used as the light source. The vibrational, rotational and other low-frequency modes in the sample will interact with photons of the laser source and cause the shift of photon energy [138]. The shift in the photon energy can provide information about molecular structure. A schematic of a Raman spectroscopy setup is shown in Figure 38.

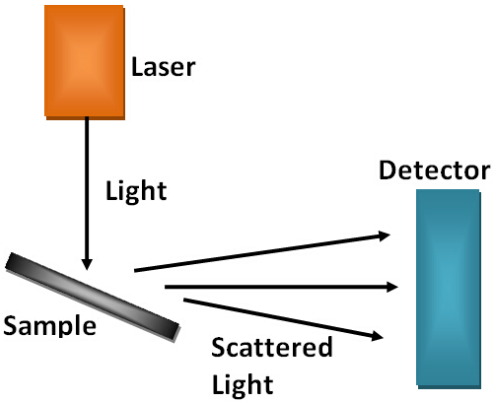

Figure 38: Schematic of Raman spectroscopy measurement

There are three main types of interactions between the photons and the sample: Stokes scattering process, anti-Stokes scattering process and Rayleigh scattering process. If the photon emitted from the sample has lower energy than the photon adsorbed, this outcome is Stokes scattering. If the emitted photon has higher energy than the absorbed photon, the process is anti-Stokes scattering. If there is no energy exchange during the scattering process, it is called Rayleigh scattering. The schematics of the three scattering processes are included in Figure 39.

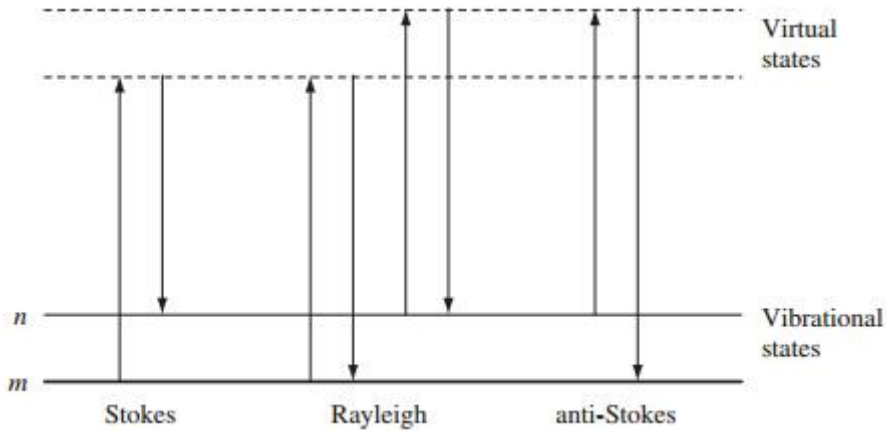

Figure 39: Schematics of three kinds of scattering processes.

Raman spectroscopy is able to probe the differences in the composition of nanotubes. For instance, amorphous carbons, carbon nanotube and graphite in the carbon composite can be distinguished by the difference of their Raman spectra. A laser with wavelength of 633 nm was used in the Raman spectroscopy experiment at ambient room temperature.

A typical Raman spectrum measurement is shown in Figure 40. The two main peaks of the Raman spectrum of the SWNTs (Sigma Aldrich) are the radial breathing mode (RBM) and G-band [139]. The RBM peak in the Raman spectrum is a low-energy phonon mode which represents the vibration of carbon atoms in the radial direction. The diameter of a SWNT is inversely proportional to the RBM frequency, expressed as $d_t = C/\omega_{RBM}$ ($C = 248\ cm^{-1} \cdot nm$). For instance, the RBM peak is at 203.6 cm^{-1} in Figure 40. This indicates that there are carbon nanotubes with diameter of 1.2 nm in the SWNT networks.

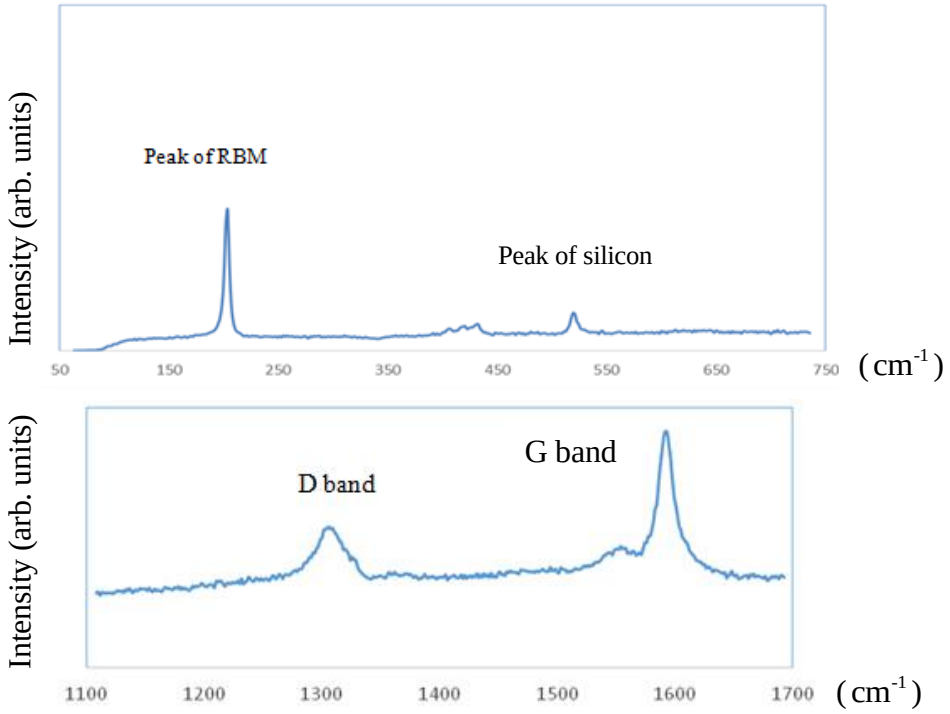

Figure 40: Raman spectroscopy of the SWNTs (RBM, G-band and D-band).

The G-band involves an optical phonon mode between carbon atoms. There are two main components of the G-band, G^+ band and G^- band. The G^+ band is associated with carbon atom vibration along the nanotube axis and it features a peak at 1590 cm^{-1}. The G^- band is associated with the vibrations of carbon atoms long the circumferential direction. The profile of G^- band can be used to distinguish metallic and semiconducting tubes. As shown in Figure 41, metallic SWNTs have more broaden lineshape of the G^- band than that of semiconducting SWNTs. The broaden G^- band lineshape of metallic tubes can be related to the presence of free electrons in metallic tubes [140]. The D-band (feature peak is ~ 1350 cm^{-1}) involves second-order Raman scattering of which phonon frequencies change with changing laser excitation energy. The D-band originates usually associated with disorder in carbon structures [139].

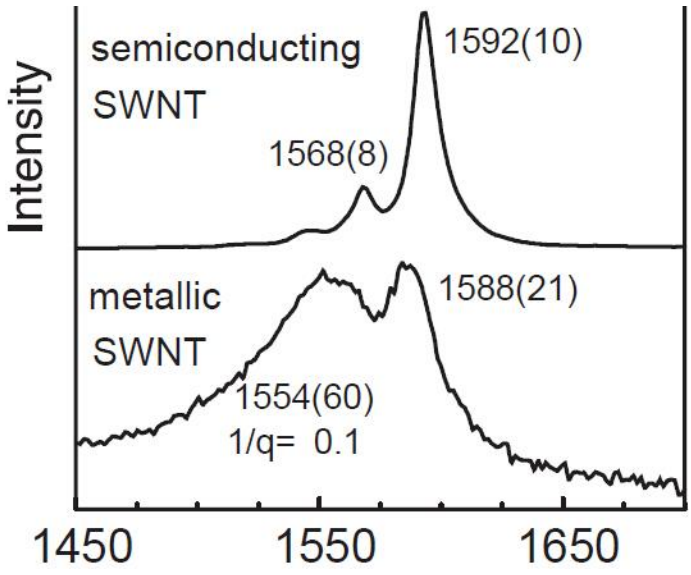

Figure 41: Examples of Raman spectroscopy of metallic and semiconducting SWNTs [139]

3.6 Summary

In summary, the properties of the patterned SWNT networks are characterized by various tools. Optical microscopy was used to examine the morphology of the colloidal sphere monolayers. It was observed that the colloidal aqueous solution (without SWNTs and surfactants) formed colloidal multilayers in the centre of the droplet and monolayers at the edge (Figure 22). Most of the colloids were deposited on the gold surface instead of silicon oxide after the evaporation of solution, due to the hydrophilic nature of the gold surface. The colloidal solutions mixed with SDS/SWNTs formed a different pattern on the substrates after its deposition (Figure 23). The colloids formed ring-like patterns with multilayer at the perimeter of the ring and colloidal monolayers formed inside the ring.

Atomic force microscopy and scanning electron microscopy were used to characterize the nanoscale structure of the patterned SWNT networks after the removal of colloidal masks. AFM images (Figure 25 and Figure 26) confirmed the formation of the ordered ring arrays. The height of the rings is about 4-10 nm and their diameter is about 400 nm. SWNTs connected between the rings were also observed. The average diameter of SWNTs bundles is 3-5 nm. In another sample, SWNT networks with mesh-like structures were observed, as shown in Figure 26. The irregularity of the ring arrays may be caused by disorder in the colloidal mask.

Two-terminal electrical conductance measurement showed that the resistance of random SWNT networks varies from device to device. Devices from sample A (dropcasting methanol–CNT solution on substrates) had resistance of 3-10 MΩ. However, no field effect behavior was observed in this sample. In contrast some random networks in sample B

(dropcasting chloroform-CNT solution on substrate) showed field effect behavior with on/off ratio of > 100. Those devices had resistance of hundreds MΩ with nonlinear I-V curve. This may be explained by the non-ideal Schottky contacts formation with the CNT channel.

The partially patterned SWNT networks (sample C, D) had resistance from ~ 20 kΩ to 10 MΩ. No field effect behavior was observed in any of these devices and likely metallic pathways are dominant in the partially patterned SWNT networks.

The two-terminal measurement (Figure 36) showed that the resistance of the fully patterned SWNT networks (sample E) is about tens of MΩ. All three devices measured showed nonlinear I-V curves. This indicated that the metal-nanotube contact was not Ohmic. The conductance of the patterned SWNT network could be modulated as a p-type transistor by varying gate voltage from -2.5V to 2.5V.

The results of Raman spectroscopy provided further information about the SWNTs in the patterned networks. The radial breathing mode peak identified the presence of SWNTs with diameter of 1.2 nm.

4 DISCUSSION AND ANALYSIS

4.1 Performance Evaluation of the Patterned SWNT Networks

In this section, the performance of the patterned SWNT networks FETs is evaluated. For a field-effect transistor, its performance can be determined by several key parameters, such as on/off ratio, carrier mobility, subthreshold slope and transconductance.

The on/off ratio of a FET device is defined as the ratio of on-state current versus off-state current. The on/off ratio of the patterned SWNT networks is summarized in Table 4. The results show that the on/off ratio of the patterned SWNT networks varies: Device 1 has highest on/off ratio (~ 10^5). However the on/off ratio of device 2 and 3 are both lower than 10. The variation of the on/off ratio in the samples is likely due to the existence of metallic SWNTs in the patterned SWNT networks, as the metallic SWNTs cannot be turned off by gate bias.

The average length of tubes (L_s) is 2 – 5 μm and the channel length of the devices (L_c) is about 2 – 7 μm. Since the L_s is comparable to L_c, there is high probability that individual tubes can bridge between the source and drain contacts. Therefore the off-state current could be significantly increased if there is metallic tube directly bridging between the contacts and would negatively affect on/off ratio.

		on/off ratio
Sample E (patterned networks)	Device 1	~ 10^5
	Device 2	~10
	Device 3	~3
Sample B (Random networks)	Device 1	~200
	Device 3	~2000

Table 4: The on/off ratio of the patterned SWNT networks and random SWNT networks

Another important parameter of a FET device is channel carrier mobility μ. The mobility represents how fast the carriers (electrons or holes) can be transported in the transistors. A generic equation to calculate the effective carrier mobility of a FET device is shown below [16]:

$$\mu_{device} = \frac{L}{V_D C_{OX} W} \frac{dI_d}{dV_g}$$

Where L is channel length, W is channel width, V_D is drain voltage, I_d is drain current, V_g is gate voltage and C_{OX} is gate capacitance.

The parallel plate model can be used to calculate the gate capacitance by using the equation $C_{OX} = \frac{\varepsilon_{ox}}{t_{ox}}$, where ε_{ox} and t_{ox} are the dielectric constant of silicon oxide and the thickness of gate dielectric, respectively [141, 142]. In this case, C_{ox} is about $6.9\times10^{-5}\ F/m^2$, given $\varepsilon_{ox} = 3.45\times10^{-11}\ F/m$ and $t_{ox} = 0.5\times10^{-6} m$.

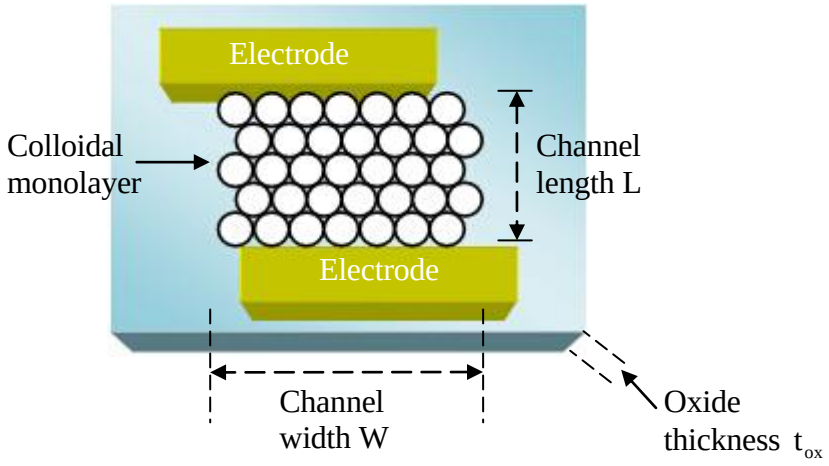

Figure 42: Illustration of the parameters of the SWNT networks

The channel width W of the patterned SWNT networks is about 28 μm, as illustrated in . The carrier mobility of the patterned SWNT networks ranges from 0.11 – 0.71 $cm^2/V \cdot s$, as shown in Table 5. In this case, the mobility results are device-specific by considering the width of the monolayer as the width of the FET channel. However, there is an overestimation of the channel width when estimating the SWNT material-specific mobility, as the area underneath colloidal monolayer is the SWNT networks with considerable spacing among the SWNT networks structures. The filling factor of the patterned SWNT networks can be calculated as

$$\text{Filling factor} = \frac{\text{Area covered by SWNTs}}{\text{Total area}}$$

According to AFM/SEM images, the filling factor F of the patterned SWNT networks is 0.132. The material-specific channel width W_m is $W_m = W \times (\text{filling factor}) = 3.7$. The material-specific mobility is calculated accordingly.

The mobility of the patterned SWNT networks is comparable to amorphous Si which is a commonly used semiconductor in thin film transistors [16]. In addition, the mobility of the patterned SWNT networks is higher than that of the organic thin film FET devices listed in Table 5.

		Mobility ($cm^2/V \cdot s$)	
		Device-specific	Material-specific
Patterned SWNT network (Sample E)	Device 1	0.23	1.74
	Device 2	0.71	5.38
	Device 3	0.11	0.83
Random SWNT network (Sample B)	Device 1	0.014	
	Device 3	0.032	
Inorganic thin film	Amorphous silicon	~1	
Organic thin film	Poly-thiophene FET	9.4×10^{-3}	
	Organic blend FET	0.01	
	Conjugated polymer FET	0.1	

Table 5: Calculated carrier mobility of the patterned SWNT networks [16, 73]. The parameter for mobility calculation of random and patterned SWNT networks are: channel length L of 2.5 – 7 µm, device channel width W of 28 µm, drain voltage V_D of 0.5 V, dielectric layer thickness of 500 nm.

The density of SWNT in the networks can be increased in order to increase its carrier mobility. There is a trade-off between the carrier mobility and the on/off ratio. With higher tube density, the carrier mobility is increased because of the increasing percolating path and less scattering. However the metallic percolating path can be increased at the same time and cause high off-state current and low on/off ratio. In order to achieve higher carrier mobility with good off state characteristics, the elimination of metallic pathway in the SWNT networks desired. For the SWNT networks made of as-grown SWNTs, the metallic

pathway in the SWNT networks can be eliminated by electrical burnout [143]. This process can be achieved by applying large source-drain voltage when turning off the semiconducting tubes with sufficient gate bias [137, 144]. By this means, the on-off ratio can be improved by five orders of magnitudes without significant loss of on-current carrying capability.

It has been observed that SWNTs form bundles in the SWNT networks, because of the strong Coulomb interaction between the tubes. Due to screening effects between the tubes, the gate modulation is less effective and device performance is degraded [145, 146]. In order to improve the patterned SWNT device performance, well-dispersed tubes in the SWNT networks are desirable.

The device performance of the patterned SWNT networks is also compared with other transistor devices made of random SWNT networks as aligned SWNT networks in Table 6.

Device 1 from sample E has on/off ratio of 10^5 which is among the best switching performance in FETs based on the SWNT networks. It indicates that there is no metallic pathway in the network of device A. The mobility of the patterned SWNT networks is about 1~2 orders of magnitude lower than typical values for FETs based on SWNT networks. This can be explained by several reasons: 1): low density of conducting pathway. 2) Low quality of SWNTs due to structural defects. 3) High resistance metal-SWNT contacts. SWNTs with enriched semiconducting tubes up to 99.5% have been used for fabricating networks to minimize the metallic path ways. Experimental results summarized in Table 6 show that enriched semiconducting SWNTs can obtain high mobility in SWNT networks while maintaining the on/off ratio.

Transconductance of the patterned SWNT networks are lower than most of the transistors based on SWNT networks, as shown in Table 6. The transconductance can be improved by optimizing the metal-tube contacts and capacitance.

		Network type	Gate type	Type of SWNTs	on/off ratio	Mobility ($cm^2/V \cdot s$)	Trans-conductance (μS)	Subthreshold slope (mV)	Tube density ($/\mu m^2$)
Sample E	Device 1	Patterned networks	backgate	As-grown	~ 10^5	0.23	0.009	~210	~1
	Device 2				~ 10	0.71	0.018	n/a	~1
	Device 3				~ 3	0.11	0.005	n/a	~1
Sample B	Device 1	Random networks	backgate	As-grown	~ 200	0.014	5.4×10^{-4}	~150	n/a
	Device 3				~ 2000	0.032	0.001	~210	n/a
	Ref [16]				~ 10^5	7	<0.05	>500	~1
	Ref [91]		Electrolyte	Enriched semiconducting tubes	~ 10^5	7.5	~50	<100	~20
	Ref [141]		backgate	As-grown	~ 10^5	>20	~2	~200	~1
	Ref [88]	Aligned networks	backgate	Enriched semiconducting tubes	~ 10^5	~6	~1	70	3
	Ref [89]		backgate	Enriched semiconducting tubes	~10^3	20	40	400	500

Table 6: Parameters of patterned SWNT network FETs. Some typical FETs based on SWNT networks in literature are also included for comparison.

4.2 Mechanism of carbon nanotube patterned network formation

In this section, the mechanism of the SWNT network formation is discussed. Colloidal lithography has been widely used as a simple and effective method for nanostructure patterning [147]. During the evaporation of the solution, the spacing between colloidal particles is decreased and a curved meniscus starts to form around the colloids [148]. Under the colloidal monolayer, the capillary forces at the solid/liquid/air interface is the driving force that push the nanoparticles to self-assemble into patterned structures [149].

Similarly, the formation of the patterned SWNT networks can be divided into several independent phases, as illustrated in Figure 43.

During the initial solution evaporation, the colloids self-assemble together due to the convective forces. Menisci start to form around the colloidal spheres due to capillary forces [147]. The SWNTs are then constrained to the area around the colloidal spheres. Since the SWNTs are flexible, the capillary force at the meniscus can push SWNTs into winding around the base of the colloids to form ring-like structures. Since the average length of SWNTs is larger than the diameter of colloids, the SWNTs can wrap between multiple colloids or form connections between SWNT rings. After the evaporation of the solution, the colloidal spheres formed closed-packed arrays and the patterned SWNT networks form ordered structures under the colloidal monolayer.

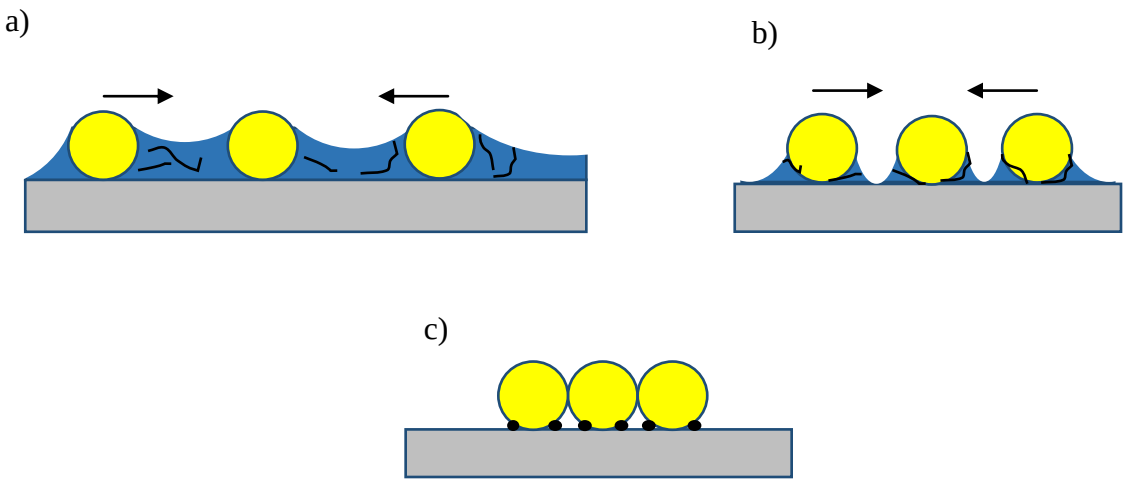

Figure 43: Schematic view of formation of the patterned SWNT networks. a) The initial stage of solution evaporation. The colloids move toward each other due to the convective forces; b) with further solution evaporation, the colloids on the substrates were move closer. The SWNTs wind around the base of the colloids due to the capillary forces; c) after the solution evaporation, the colloids form closed packed monolayer. The SWNTs formed patterned structures under the colloidal monolayer.

In this work, patterned SWNT networks are for the first time formed via solution deposition on a heterogeneous surface. The hydrophobic SiO_2/Si substrates are partially covered by gold pads and electrodes. According to the SEM and AFM results, the SWNT rings formed on SiO_2 and gold surface have no qualitative significant morphology difference. Not all the SWNT rings are interconnected by SWNT to form conducting networks. In Table 7, the percentage of SWNT rings which has interconnects with at least one connection with other rings is counted, based on SEM results in 6 different locations. On average, 13% of SWNT rings on SiO_2 surface have connections with other rings, while 40% of SWNT rings on gold interconnect with other rings. This statistical result indicates that the throughput of SWNT ring interconnections on a gold surface is higher than that on a SiO_2 surface.

location	# of rings on silicon oxide	# of rings on SiO_2 has interconnection	percentage	# of rings on gold	# of rings on gold has interconnection	percentage
03	468	49	**10%**	227	73	32%
04	492	66	13%	91	42	46%
05	91	13	14%	53	33	62%
11	49	2	4%	92	22	24%
12	54	21	39%	109	59	54%
14	171	27	16%	N/A	N/A	N/A
Total	**1325**	**178**	**Avg. 13%**	**572**	**229**	**Avg. 40%**

Table 7: Percentage of SWNT rings forming networks is summarized. Data from six different locations of the SEM images is included, according to SEM result (Figure 28 and Figure 29). Note: location 14 include SiO_2 surface only.

5 CONCLUSION AND FUTURE WORK

5.1 Summary

In this thesis, the fabrication process of patterned SWNT networks has been investigated along with its structural and electrical properties. For the first time, the patterned SWNT networks were fabricated on a heterogeneous surface and the field effect characteristic as FET devices were measured. A simple and straight-forward method of patterning SWNT networks is developed by depositing SWNTs from solution onto a self-assembled colloidal mask. The colloidal masks were composed of colloidal monolayer sphere monolayer, which can be obtained by depositing aqueous colloidal solution on substrates. Two kinds of colloids (polystyrene spheres with diameter of 780 nm and silica spheres with diameter of 800 nm) were used to fabricate the masks. It was found that there is an optimal concentration of colloidal solution (0.02 wt% ~ 0.04 wt% for polystyrene spheres and 0.025 wt% ~ 0.05 wt% for silica spheres) in order to maximize the creation of colloidal monolayers. Colloidal solution with higher concentration will increase the output of colloidal multilayer, as the excessive colloids stack up. More diluted colloidal solutions however have insufficient colloids to form a monolayer.

The morphology of the patterned SWNT networks was characterized by AFM and SEM after the removal of the colloidal mask. It was found that SWNTs can form an ordered array of interconnected SWNT rings. The diameter of the rings is about 400 nm and its height is about 4-10 nm. Mesh-like structures of SWNT networks were also observed.

The electrical properties of the patterned SWNT networks were characterized under ambient condition. Two terminal measurements showed that the resistance of the patterned

SWNT networks is about tens of MΩ. It is assumed that the non-ideal Schottky barrier at gold-nanotube contact caused high contact resistance. By applying a back-gate bias, the field-effect characteristics of the patterned networks were measured. The patterned SWNT networks behaved as p-type field effect transistors. The highest on/off ratio obtained is about 10^5 which satisfy the requirements for transistor logic application. Some samples have on/off less than 10. The lower on/off ratio is likely caused by the metallic pathway in the SWNT networks. The highest mobility of the devices achieved in this work is 0.71 $cm^2/V \cdot s$, which outperformed most organic thin film transistors (Table 5).

5.2 Future Work

Future work should include the optimization of the fabrication process to improve the yield of the patterned SWNT networks and performance enhancement of the patterned SWNT networks as FET devices. In addition, different device structures and application based on patterned SWNT networks can be explored

5.2.1 Optimizing fabrication process of the patterned SWNT networks

Experimental results in this work have shown that the throughput of the patterned SWNT networks is relatively low. Though SWNT rings can be patterned over a large area in an ordered fashion, not all rings are interconnected. It is observed that more SWNT rings on a gold surface are interconnected than that on silicon oxide. This implies that the output of the patterned SWNT networks can be increased by using substrates with a hydrophilic surface. For example, mica or polymer (for example, poly(ethylene terephthalate)) can be used in order to increase the throughput of the patterned SWNT networks [150]. When the colloidal monolayer is removed, SWNTs in the patterned networks underneath the colloids

could be also removed. This may be because SWNTs are more adhesive to colloids rather than the surface of the substrates. Therefore, if SWNTs can be modified (for instance, surface modification) to be more sticky to the substrate, the output of the patterned SWNT networks can be significantly increased. The same process can also be applied to the substrate (i.e., surface modified).

In this work, only the patterned SWNT networks lying across two pre-defined gold electrodes are measured. Thus, few SWNT networks qualify for electrical measurement. In order to measure more patterned SWNT networks, one method is proposed as shown in Figure 44. Firstly, the SEM and AFM tools are used to locate the patterned SWNT networks on the substrates. Subsequently, the source/drain contacts and top-gates can be fabricated on the patterned SWNT network via lithography technique.

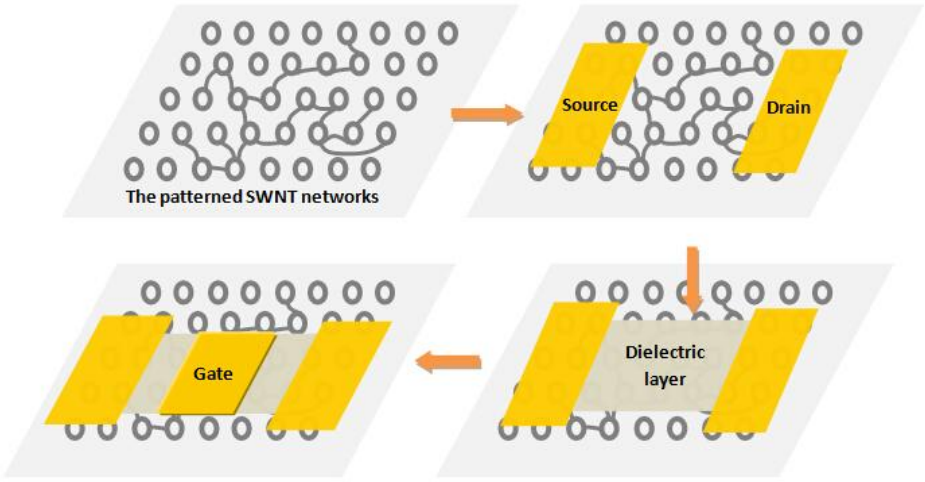

Figure 44: Schematic of measuring the patterned SWNT networks without predefined electrodes: a) Locate the patterned SWNT networks by AFM/SEM; b) Fabrication of drain and source electrodes; c) Fabrication of dielectric layer on top of the patterned SWNT networks; d) Fabrication of top-gate electrode

5.2.2 Device performance enhancement and future applications

Future work can also include improving the device performance of the patterned SWNT networks. Metallic pathways seem to exist in some of the devices measured in this work. As a result, the FET device performance, especially the on/off ratio is deteriorated. It is hypothesized that the on/off ratio of the patterned SWNT networks can be significantly improved by using the highly purified semiconducting tubes instead of the as-grown ones. In order to reduce the resistance of SWNT-tube contacts, metals with proper work function (such as palladium) can be used as electrodes instead of gold. The backgate used in this work provides relatively weak electrostatic control over the channel of the FET devices. Top-gate or dual gate configuration with high-k dielectrics can be used to enhance the switching performance of the FET devices.

The potential applications of the patterned SWNT networks include transparent electronics, flexible electronics and sensor applications. The transparency of SWNT networks can reach up to 90% [77, 151]. Highly transparent SWNT networks could be widely used in transparent electrode applications. If the patterned SWNT networks can be fabricated on a large scale, it may outperform the conductive thin film made of random SWNT networks assessed in previous work [77, 151]. Electronics on mechanically flexible substrates are also very promising for potential applications in consumer electronics and medical devices [152, 153]. By properly modifying the sidewall of SWNT, the patterned SWNT networks can be useful for sensing applications, due to their large active surface area.

a)

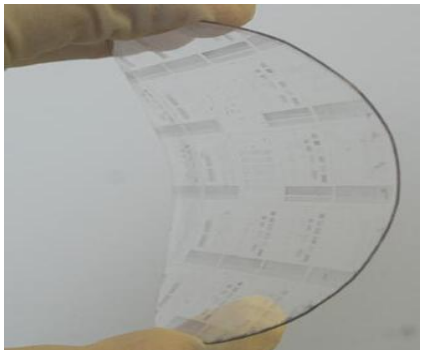

b)

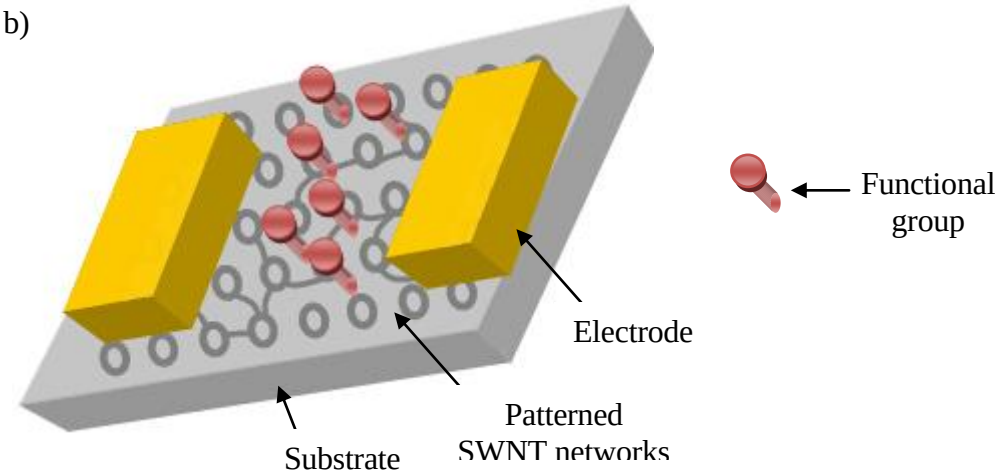

Figure 45: Schematics of some potential device structures based on patterned SWNT networks: a) transparent and flexible electronics [154]; b) sensor applications

Colloidal lithography is a simple and versatile tool for nanostructure patterning, not only for SWNTs, but also for other nanoparticles. The experiments described in this thesis could be a valuable platform for studying general nanostructure patterning as well as in the electrical characterization.

6 BIBLIOGRAPHY

[1] S. Iijima, "Helical microtubules of graphitic carbon," *Nature*, vol. 354, pp. 56-58, 11/07/print 1991.

[2] D. Bethune, C. Klang, M. De Vries, G. Gorman, R. Savoy, J. Vazquez, *et al.*, "Cobalt-catalysed growth of carbon nanotubes with single-atomic-layer walls," 1993.

[3] S. Gullapalli and M. S. Wong, "Nanotechnology: a guide to nano-objects," *Chemical Engineering Progress*, vol. 107, pp. 28-32, 2011.

[4] E. Pop, D. Mann, Q. Wang, K. Goodson, and H. Dai, "Thermal conductance of an individual single-wall carbon nanotube above room temperature," *Nano Letters*, vol. 6, pp. 96-100, 2006.

[5] B. Gao, A. Kleinhammes, X. Tang, C. Bower, L. Fleming, Y. Wu, *et al.*, "Electrochemical intercalation of single-walled carbon nanotubes with lithium," *Chemical Physics Letters*, vol. 307, pp. 153-157, 1999.

[6] K. H. An, W. S. Kim, Y. S. Park, J.-M. Moon, D. J. Bae, S. C. Lim, *et al.*, "Electrochemical properties of high-power supercapacitors using single-walled carbon nanotube electrodes," *Advanced Functional Materials*, vol. 11, pp. 387-392, 2001.

[7] C. Nanotubes, "Advanced Topics in the Synthesis, Structure, Properties and Applications," *Topics in applied physics*, vol. 111, p. 353À369, 2008.

[8] C. Wang, M. Waje, X. Wang, J. M. Tang, R. C. Haddon, and Y. Yan, "Proton exchange membrane fuel cells with carbon nanotube based electrodes," *Nano letters*, vol. 4, pp. 345-348, 2004.

[9] C. Dekker, "Carbon nanotubes as molecular quantum wires," *Physics today*, vol. 52, pp. 22-30, 1999.

[10] A. Javey, J. Guo, Q. Wang, M. Lundstrom, and H. Dai, "Ballistic carbon nanotube field-effect transistors," *Nature*, vol. 424, pp. 654-657, 2003.

[11] M. F. De Volder, S. H. Tawfick, R. H. Baughman, and A. J. Hart, "Carbon nanotubes: present and future commercial applications," *Science*, vol. 339, pp. 535-539, 2013.

[12] P. Avouris, R. Martel, V. Derycke, and J. Appenzeller, "Carbon nanotube transistors and logic circuits," *Physica B: Condensed Matter*, vol. 323, pp. 6-14, 2002.

[13] A. D. Franklin, M. Luisier, S.-J. Han, G. Tulevski, C. M. Breslin, L. Gignac, *et al.*, "Sub-10 nm carbon nanotube transistor," *Nano letters,* vol. 12, pp. 758-762, 2012.

[14] S. Park, M. Vosguerichian, and Z. Bao, "A review of fabrication and applications of carbon nanotube film-based flexible electronics," *Nanoscale,* vol. 5, pp. 1727-1752, 2013.

[15] S. J. Kang, C. Kocabas, T. Ozel, M. Shim, N. Pimparkar, M. A. Alam, *et al.*, "High-performance electronics using dense, perfectly aligned arrays of single-walled carbon nanotubes," *Nature Nanotechnology,* vol. 2, pp. 230-236, 2007.

[16] E. Snow, J. Novak, P. Campbell, and D. Park, "Random networks of carbon nanotubes as an electronic material," *Applied Physics Letters,* vol. 82, pp. 2145-2147, 2003.

[17] P. Qi, O. Vermesh, M. Grecu, A. Javey, Q. Wang, H. Dai, *et al.*, "Toward large arrays of multiplex functionalized carbon nanotube sensors for highly sensitive and selective molecular detection," *Nano Letters,* vol. 3, pp. 347-351, 2003.

[18] G. Gruner, "Carbon nanotube transistors for biosensing applications," *Analytical and bioanalytical chemistry,* vol. 384, pp. 322-335, 2006.

[19] G. Gruner, "Carbon nanotube films for transparent and plastic electronics," *J. Mater. Chem.,* vol. 16, pp. 3533-3539, 2006.

[20] E. Artukovic, M. Kaempgen, D. Hecht, S. Roth, and G. Grüner, "Transparent and flexible carbon nanotube transistors," *Nano Letters,* vol. 5, pp. 757-760, 2005.

[21] T. W. Odom, J.-L. Huang, P. Kim, and C. M. Lieber, "Structure and Electronic Properties of Carbon Nanotubes," *The Journal of Physical Chemistry B,* vol. 104, pp. 2794-2809, 2000/04/01 2000.

[22] R. Saito, G. Dresselhaus, and M. S. Dresselhaus, *Physical properties of carbon nanotubes* vol. 4: World Scientific, 1998.

[23] R. D. Booker and E. Boysen, *Nanotechnology for dummies*: John Wiley & Sons, 2011.

[24] N. Hamada, S.-i. Sawada, and A. Oshiyama, "New one-dimensional conductors: Graphitic microtubules," *Physical Review Letters,* vol. 68, pp. 1579-1581, 1992.

[25] J. W. Mintmire, B. I. Dunlap, and C. T. White, "Are fullerene tubules metallic?," *Physical Review Letters,* vol. 68, pp. 631-634, 1992.

[26] R. Saito, G. Dresselhaus, and M. S. Dresselhaus, *Physical properties of carbon nanotubes* vol. 35: World Scientific, 1998.

[27] T. S. Jespersen, "Raman Scattering in Carbon Nanotubes," Master thesis, Niels Bohr Institute, Copenhagen University, 2003.

[28] P. L. McEuen, M. S. Fuhrer, and H. Park, "Single-walled carbon nanotube electronics," *Nanotechnology, IEEE Transactions on,* vol. 1, pp. 78-85, 2002.

[29] C. T. White and T. N. Todorov, "Carbon nanotubes as long ballistic conductors," *Nature,* vol. 393, pp. 240-242, 1998.

[30] A. Jorio, G. Dresselhaus, and M. S. Dresselhaus, *Carbon nanotubes: advanced topics in the synthesis, structure, properties and applications* vol. 111: Springer, 2008.

[31] A. Jorio, G. Dresselhaus, and M. S. Dresselhaus, *Carbon nanotubes: advanced topics in the synthesis, structure, properties and applications* vol. 111: Springer, 2007.

[32] T. Ando and T. Nakanishi, "Impurity scattering in carbon nanotubes-Absence of back scattering," *Journal of the Physical Society of Japan,* vol. 67, pp. 1704-1713, 1998.

[33] P. L. McEuen, M. Bockrath, D. H. Cobden, Y. G. Yoon, and S. G. Louie, "Disorder, pseudospins, and backscattering in carbon nanotubes," *Physical Review Letters,* vol. 83, pp. 5098-5101, 1999.

[34] J. Y. Park, S. Rosenblatt, Y. Yaish, V. Sazonova, H. Üstünel, S. Braig, *et al.*, "Electron-phonon scattering in metallic single-walled carbon nanotubes," *Nano Letters,* vol. 4, pp. 517-520, 2004.

[35] F. Schwierz, "Graphene transistors," *Nature Nanotechnology,* vol. 5, pp. 487-496, 2010.

[36] S. M. Sze and K. K. Ng, *Physics of semiconductor devices*: John Wiley & Sons, 2006.

[37] S. Morozov, K. Novoselov, M. Katsnelson, F. Schedin, D. Elias, J. Jaszczak, *et al.*, "Giant intrinsic carrier mobilities in graphene and its bilayer," *Physical Review Letters,* vol. 100, p. 016602, 2008.

[38] J.-H. Chen, C. Jang, S. Xiao, M. Ishigami, and M. S. Fuhrer, "Intrinsic and extrinsic performance limits of graphene devices on SiO2," *Nature Nanotechnology,* vol. 3, pp. 206-209, 2008.

[39] T. Ohta, A. Bostwick, T. Seyller, K. Horn, and E. Rotenberg, "Controlling the electronic structure of bilayer graphene," *Science,* vol. 313, pp. 951-954, 2006.

[40] X. Peng and R. Ahuja, "Symmetry breaking induced bandgap in epitaxial graphene layers on SiC," *Nano Letters,* vol. 8, pp. 4464-4468, 2008.

[41] V. M. Pereira, A. H. Castro Neto, and N. M. R. Peres, "Tight-binding approach to uniaxial strain in graphene," *Physical Review B,* vol. 80, p. 045401, 2009.

[42] Z. H. Ni, T. Yu, Y. H. Lu, Y. Y. Wang, Y. P. Feng, and Z. X. Shen, "Uniaxial Strain on Graphene: Raman Spectroscopy Study and Band-Gap Opening," *Acs Nano,* vol. 2, pp. 2301-2305, 2008/11/25 2008.

[43] S. Zhou, G.-H. Gweon, A. Fedorov, P. First, W. De Heer, D.-H. Lee, *et al.*, "Substrate-induced bandgap opening in epitaxial graphene," *Nature materials,* vol. 6, pp. 770-775, 2007.

[44] J. B. Oostinga, H. B. Heersche, X. Liu, A. F. Morpurgo, and L. M. Vandersypen, "Gate-induced insulating state in bilayer graphene devices," *Nature materials,* vol. 7, pp. 151-157, 2007.

[45] P. Gallagher, K. Todd, and D. Goldhaber-Gordon, "Disorder-induced gap behavior in graphene nanoribbons," *Physical Review B,* vol. 81, p. 115409, 2010.

[46] C. Stampfer, J. Güttinger, S. Hellmüller, F. Molitor, K. Ensslin, and T. Ihn, "Energy gaps in etched graphene nanoribbons," *Physical review letters,* vol. 102, p. 056403, 2009.

[47] T. Shimizu, J. Haruyama, D. Marcano, D. Kosinkin, J. Tour, K. Hirose, *et al.*, "Large intrinsic energy bandgaps in annealed nanotube-derived graphene nanoribbons," *Nature nanotechnology,* vol. 6, pp. 45-50, 2011.

[48] L. Tapaszto, G. Dobrik, P. Lambin, and L. P. Biro, "Tailoring the atomic structure of graphene nanoribbons by scanning tunnelling microscope lithography," *Nature Nanotechnology,* vol. 3, pp. 397-401, 2008.

[49] J. Cai, P. Ruffieux, R. Jaafar, M. Bieri, T. Braun, S. Blankenburg, *et al.*, "Atomically precise bottom-up fabrication of graphene nanoribbons," *Nature,* vol. 466, pp. 470-473, 2010.

[50] M. Y. Han, B. Özyilmaz, Y. Zhang, and P. Kim, "Energy band-gap engineering of graphene nanoribbons," *Physical Review Letters,* vol. 98, p. 206805, 2007.

[51] B. Obradovic, R. Kotlyar, F. Heinz, P. Matagne, T. Rakshit, M. Giles, *et al.*, "Analysis of graphene nanoribbons as a channel material for field-effect transistors," *Applied Physics Letters,* vol. 88, pp. 142102-142102-3, 2006.

[52] T. Fang, A. Konar, H. Xing, and D. Jena, "Mobility in semiconducting graphene nanoribbons: Phonon, impurity, and edge roughness scattering," *Physical Review B,* vol. 78, p. 205403, 2008.

[53] A. D. Franklin and Z. Chen, "Length scaling of carbon nanotube transistors," *Nature Nanotechnology,* vol. 5, pp. 858-862, 2010.

[54] R. Martel, T. Schmidt, H. Shea, T. Hertel, and P. Avouris, "Single-and multi-wall carbon nanotube field-effect transistors," *Applied Physics Letters,* vol. 73, pp. 2447-2449, 1998.

[55] S. J. Tans, A. R. Verschueren, and C. Dekker, "Room-temperature transistor based on a single carbon nanotube," *Nature,* vol. 393, pp. 49-52, 1998.

[56] J.-P. Colinge and C. A. Colinge, *Physics of semiconductor devices*: Springer, 2005.

[57] S. Sze, "Physics of semiconductor devices. 1981," ed: Wiley, New York, 1981.

[58] A. Javey, H. Kim, M. Brink, Q. Wang, A. Ural, J. Guo, *et al.*, "High-κ dielectrics for advanced carbon-nanotube transistors and logic gates," *Nature materials,* vol. 1, pp. 241-246, 2002.

[59] A. Javey, J. Guo, D. B. Farmer, Q. Wang, D. Wang, R. G. Gordon, *et al.*, "Carbon nanotube field-effect transistors with integrated ohmic contacts and high-κ gate dielectrics," *Nano Letters,* vol. 4, pp. 447-450, 2004.

[60] Y.-M. Lin, J. Appenzeller, Z. Chen, Z.-G. Chen, H.-M. Cheng, and P. Avouris, "High-performance dual-gate carbon nanotube FETs with 40-nm gate length," *Electron Device Letters, IEEE,* vol. 26, pp. 823-825, 2005.

[61] A. Javey, J. Guo, D. B. Farmer, Q. Wang, E. Yenilmez, R. G. Gordon, *et al.*, "Self-aligned ballistic molecular transistors and electrically parallel nanotube arrays," *Nano letters,* vol. 4, pp. 1319-1322, 2004.

[62] R. Martel, V. Derycke, C. Lavoie, J. Appenzeller, K. Chan, J. Tersoff, *et al.*, "Ambipolar electrical transport in semiconducting single-wall carbon nanotubes," *Physical Review Letters,* vol. 87, p. 256805, 2001.

[63] S. Heinze, J. Tersoff, R. Martel, V. Derycke, J. Appenzeller, and P. Avouris, "Carbon nanotubes as Schottky barrier transistors," *Physical Review Letters,* vol. 89, p. 106801, 2002.

[64] J. Appenzeller, J. Knoch, V. Derycke, R. Martel, S. Wind, and P. Avouris, "Field-modulated carrier transport in carbon nanotube transistors," *Physical Review Letters,* vol. 89, p. 126801, 2002.

[65] Z. Zhang, X. Liang, S. Wang, K. Yao, Y. Hu, Y. Zhu, *et al.*, "Doping-free fabrication of carbon nanotube based ballistic CMOS devices and circuits," *Nano Letters,* vol. 7, pp. 3603-3607, 2007.

[66] L. Ding, S. Wang, Z. Zhang, Q. Zeng, Z. Wang, T. Pei, *et al.*, "Y-contacted high-performance n-type single-walled carbon nanotube field-effect transistors: scaling and comparison with Sc-contacted devices," *Nano letters,* vol. 9, pp. 4209-4214, 2009.

[67] Z. Chen, J. Appenzeller, J. Knoch, Y.-m. Lin, and P. Avouris, "The role of metal-nanotube contact in the performance of carbon nanotube field-effect transistors," *Nano Letters,* vol. 5, pp. 1497-1502, 2005.

[68] J. Appenzeller, "Carbon nanotubes for high-performance electronics—progress and prospect," *Proceedings of the IEEE,* vol. 96, pp. 201-211, 2008.

[69] Q. Cao and S.-j. Han, "Single-walled carbon nanotubes for high-performance electronics," *Nanoscale,* vol. 5, pp. 8852-8863, 2013.

[70] A. D. Franklin, R. A. Sayer, T. D. Sands, T. S. Fisher, and D. B. Janes, "Toward surround gates on vertical single-walled carbon nanotube devices," *Journal of Vacuum Science & Technology B,* vol. 27, pp. 821-826, 2009.

[71] Z. Chen, D. Farmer, S. Xu, R. Gordon, P. Avouris, and J. Appenzeller, "Externally assembled gate-all-around carbon nanotube field-effect transistor," 2008.

[72] M. Y. Timmermans, D. Estrada, A. G. Nasibulin, J. D. Wood, A. Behnam, D.-m. Sun, *et al.,* "Effect of carbon nanotube network morphology on thin film transistor performance," *Nano Research,* vol. 5, pp. 307-319, 2012.

[73] M. Shiraishi, T. Takenobu, T. Iwai, Y. Iwasa, H. Kataura, and M. Ata, "Single-walled carbon nanotube aggregates for solution-processed field effect transistors," *Chemical physics letters,* vol. 394, pp. 110-113, 2004.

[74] K. Choi, J. Bourgoin, S. Auvray, D. Esteve, G. Duesberg, S. Roth, *et al.*, "Controlled deposition of carbon nanotubes on a patterned substrate," *Surface science,* vol. 462, pp. 195-202, 2000.

[75] J. Liu, M. J. Casavant, M. Cox, D. Walters, P. Boul, W. Lu, *et al.,* "Controlled deposition of individual single-walled carbon nanotubes on chemically functionalized templates," *Chemical physics letters,* vol. 303, pp. 125-129, 1999.

[76] Y. Kim, N. Minami, W. Zhu, S. Kazaoui, R. Azumi, and M. Matsumoto, "Langmuir-Blodgett films of single-wall carbon nanotubes: layer-by-layer deposition and in-plane orientation of tubes," *JAPANESE JOURNAL OF APPLIED PHYSICS PART 1 REGULAR PAPERS SHORT NOTES AND REVIEW PAPERS,* vol. 42, pp. 7629-7634, 2003.

[77] L. Hu, D. Hecht, and G. Grüner, "Percolation in transparent and conducting carbon nanotube networks," *Nano Letters,* vol. 4, pp. 2513-2517, 2004.

[78] Z. Wu, Z. Chen, X. Du, J. M. Logan, J. Sippel, M. Nikolou, *et al.*, "Transparent, conductive carbon nanotube films," *Science,* vol. 305, pp. 1273-1276, 2004.

[79] Q. Wang and H. Moriyama, "Carbon Nanotube-Based Thin Films: Synthesis and Properties."

[80] J. U. Park, M. Meitl, S. H. Hur, M. L. Usrey, M. S. Strano, P. J. A. Kenis, *et al.*, "In Situ Deposition and Patterning of Single‐Walled Carbon Nanotubes by Laminar Flow and Controlled Flocculation in Microfluidic Channels," *Angewandte Chemie*, vol. 118, pp. 595-599, 2005.

[81] M. A. Meitl, Y. Zhou, A. Gaur, S. Jeon, M. L. Usrey, M. S. Strano, *et al.*, "Solution casting and transfer printing single-walled carbon nanotube films," *Nano Letters*, vol. 4, pp. 1643-1647, 2004.

[82] Q. Cao and J. A. Rogers, "Ultrathin Films of Single‐Walled Carbon Nanotubes for Electronics and Sensors: A Review of Fundamental and Applied Aspects," *Advanced Materials*, vol. 21, pp. 29-53, 2009.

[83] S. Maruyama, R. Kojima, Y. Miyauchi, S. Chiashi, and M. Kohno, "Low-temperature synthesis of high-purity single-walled carbon nanotubes from alcohol," *Chemical physics letters*, vol. 360, pp. 229-234, 2002.

[84] Q. Cao, S. H. Hur, Z. T. Zhu, Y. Sun, C. J. Wang, M. A. Meitl, *et al.*, "Highly Bendable, Transparent Thin‐Film Transistors That Use Carbon‐Nanotube‐Based Conductors and Semiconductors with Elastomeric Dielectrics," *Advanced Materials*, vol. 18, pp. 304-309, 2006.

[85] R. Seidel, A. P. Graham, E. Unger, G. S. Duesberg, M. Liebau, W. Steinhoegl, *et al.*, "High-Current Nanotube Transistors," *Nano Letters*, vol. 4, pp. 831-834, 2004/05/01 2004.

[86] J. Kong, H. T. Soh, A. M. Cassell, C. F. Quate, and H. Dai, "Synthesis of individual single-walled carbon nanotubes on patterned silicon wafers," *Nature*, vol. 395, pp. 878-881, 1998.

[87] N. R. Franklin and H. Dai, "An enhanced CVD approach to extensive nanotube networks with directionality," *Advanced Materials*, vol. 12, pp. 890-894, 2000.

[88] A. D. Franklin, A. Lin, H.-S. Wong, and Z. Chen, "Current scaling in aligned carbon nanotube array transistors with local bottom gating," *Electron Device Letters, IEEE*, vol. 31, pp. 644-646, 2010.

[89] Q. Cao, S.-j. Han, G. S. Tulevski, Y. Zhu, D. D. Lu, and W. Haensch, "Arrays of single-walled carbon nanotubes with full surface coverage for high-performance electronics," *Nature Nanotechnology*, vol. 8, pp. 180-186, 2013.

[90] J. Wu, L. Jiao, A. Antaris, C. L. Choi, L. Xie, Y. Wu, *et al.*, "Self‐Assembly of Semiconducting Single‐Walled Carbon Nanotubes into Dense, Aligned Rafts," *Small*, vol. 9, pp. 4142-4148, 2013.

[91] J. Zaumseil, F. Jakubka, M. Wang, and F. Gannott, "In Situ Raman Mapping of Charge Carrier Distribution in Electrolyte-Gated Carbon Nanotube Network Field-

Effect Transistors," *The Journal of Physical Chemistry C,* vol. 117, pp. 26361-26370, 2013.

[92] S. Z. Bisri, J. Gao, V. Derenskyi, W. Gomulya, I. Iezhokin, P. Gordiichuk, *et al.*, "High Performance Ambipolar Field‐Effect Transistor of Random Network Carbon Nanotubes," *Advanced Materials,* vol. 24, pp. 6147-6152, 2012.

[93] T. Zhang, S. Mubeen, N. V. Myung, and M. A. Deshusses, "Recent progress in carbon nanotube-based gas sensors," *Nanotechnology,* vol. 19, p. 332001, 2008.

[94] J. Li, Y. Lu, Q. Ye, M. Cinke, J. Han, and M. Meyyappan, "Carbon nanotube sensors for gas and organic vapor detection," *Nano Letters,* vol. 3, pp. 929-933, 2003.

[95] S. J. Oh, J. Zhang, Y. Cheng, H. Shimoda, and O. Zhou, "Liquid-phase fabrication of patterned carbon nanotube field emission cathodes," *Applied Physics Letters,* vol. 84, pp. 3738-3740, 2004.

[96] Y. Chen and C. Papadopoulos, "Patterned single-walled carbon nanotube network field-effect transistors," presented at the 15th Canadian Semiconductor Science and Technology Conference, Vancouver, 2011.

[97] Y. Chen and C. Papadopoulos, "Patterned carbon nanotube FET channels," *in preparation,* 2014.

[98] S.-M. Yang, S. G. Jang, D.-G. Choi, S. Kim, and H. K. Yu, "Nanomachining by Colloidal Lithography," *Small,* vol. 2, pp. 458-475, 2006.

[99] P. J. Silverman, "The Intel Lithography Roadmap," *Intel Technology Journal,* vol. 6, p. 55, 2002.

[100] C. L. Haynes and R. P. Van Duyne, "Nanosphere Lithography: A Versatile Nanofabrication Tool for Studies of Size-Dependent Nanoparticle Optics," *The Journal of Physical Chemistry B,* vol. 105, pp. 5599-5611, 2001/06/01 2001.

[101] T. Ito and S. Okazaki, "Pushing the limits of lithography," *Nature,* vol. 406, pp. 1027-1031, 2000.

[102] L. J. Guo, "Nanoimprint lithography: methods and material requirements," *Advanced Materials,* vol. 19, pp. 495-513, 2007.

[103] U. C. Fischer and H. P. Zingsheim, *Submicroscopic pattern replication with visible light* vol. 19: AVS, 1981.

[104] H. W. Deckman and J. H. Dunsmuir, *Natural lithography* vol. 41: AIP, 1982.

[105] A. Kosiorek, W. Kandulski, H. Glaczynska, and M. Giersig, "Fabrication of Nanoscale Rings, Dots, and Rods by Combining Shadow Nanosphere Lithography and Annealed Polystyrene Nanosphere Masks," *Small,* vol. 1, pp. 439-444, 2005.

[106] J. Zhang, Y. Li, X. Zhang, and B. Yang, "Colloidal Self-Assembly Meets Nanofabrication: From Two-Dimensional Colloidal Crystals to Nanostructure Arrays," *Advanced Materials,* vol. 22, pp. 4249-4269, 2010.

[107] I. U. Vakarelski, D. Y. C. Chan, T. Nonoguchi, H. Shinto, and K. Higashitani, "Assembly of Gold Nanoparticles into Microwire Networks Induced by Drying Liquid Bridges," *Physical Review Letters,* vol. 102, p. 058303, 2009.

[108] Z. Chen, Y.-M. Lin, M. J. Rooks, and P. Avouris, "Graphene nano-ribbon electronics," *Physica E: Low-dimensional Systems and Nanostructures,* vol. 40, pp. 228-232, 2007.

[109] C. Dionigi, P. Stoliar, G. Ruani, S. D. Quiroga, M. Facchini, and F. Biscarini, "Carbon nanotube networks patterned from aqueous solutions of latex bead carriers," *Journal of Materials Chemistry,* vol. 17, pp. 3681-3686, 2007.

[110] F. Sun, W. Cai, Y. Li, B. Cao, Y. Lei, and L. Zhang, "Morphology-Controlled Growth of Large-Area Two-Dimensional Ordered Pore Arrays," *Advanced Functional Materials,* vol. 14, pp. 283-288, 2004.

[111] J. Boneberg, F. Burmeister, C. Schäfle, P. Leiderer, D. Reim, A. Fery, *et al.*, "The Formation of Nano-Dot and Nano-Ring Structures in Colloidal Monolayer Lithography†," *Langmuir,* vol. 13, pp. 7080-7084, 1997/12/01 1997.

[112] A. S. Dimitrov and K. Nagayama, "Continuous Convective Assembling of Fine Particles into Two-Dimensional Arrays on Solid Surfaces," *Langmuir,* vol. 12, pp. 1303-1311, 1996/01/01 1996.

[113] G. A. Ozin and S. M. Yang, "The Race for the Photonic Chip: Colloidal Crystal Assembly in Silicon Wafers," *Advanced Functional Materials,* vol. 11, pp. 95-104, 2001.

[114] X. M. Lin, H. M. Jaeger, C. M. Sorensen, and K. J. Klabunde, "Formation of Long-Range-Ordered Nanocrystal Superlattices on Silicon Nitride Substrates," *The Journal of Physical Chemistry B,* vol. 105, pp. 3353-3357, 2001/05/01 2001.

[115] S. Narayanan, J. Wang, and X.-M. Lin, "Dynamical Self-Assembly of Nanocrystal Superlattices during Colloidal Droplet Evaporation by in situ Small Angle X-Ray Scattering," *Physical Review Letters,* vol. 93, p. 135503, 2004.

[116] R. R. Thomas, F. B. Kaufman, J. T. Kirleis, and R. A. Belsky, "Wettability of Polished Silicon Oxide Surfaces," *Journal of The Electrochemical Society,* vol. 143, pp. 643-648, 1996.

[117] S. Malcolm E, "Wettability of clean metal surfaces," *Journal of Colloid and Interface Science,* vol. 100, pp. 372-380, 1984.

[118] H. Asoh, S. Sakamoto, and S. Ono, "Metal patterning on silicon surface by site-selective electroless deposition through colloidal crystal templating," *Journal of Colloid and Interface Science,* vol. 316, pp. 547-552, 2007.

[119] I. Jurewicz, P. Worajittiphon, A. A. K. King, P. J. Sellin, J. L. Keddie, and A. B. Dalton, "Locking Carbon Nanotubes in Confined Lattice Geometries − A Route to Low Percolation in Conducting Composites," *The Journal of Physical Chemistry B,* vol. 115, pp. 6395-6400, 2011/05/26 2011.

[120] M. H. Kim, J. Y. Choi, H. K. Choi, S. M. Yoon, O. O. Park, D. K. Yi, *et al.*, "Carbon Nanotube Network Structuring Using Two-Dimensional Colloidal Crystal Templates," *Advanced Materials,* vol. 20, pp. 457-461, 2008.

[121] D. K. Yi, J.-H. Lee, J. A. Rogers, and U. Paik, *Two-dimensional nanohybridization of gold nanorods and polystyrene colloids* vol. 94: AIP, 2009.

[122] C.-X. Liu and J.-W. Choi, "Improved dispersion of carbon nanotubes in polymers at high concentrations," *Nanomaterials,* vol. 2, pp. 329-347, 2012.

[123] Y. Wang, Z. Iqbal, and S. Mitra, "Rapidly functionalized, water-dispersed carbon nanotubes at high concentration," *Journal of the American Chemical Society,* vol. 128, pp. 95-99, 2006.

[124] L. Vaisman, H. D. Wagner, and G. Marom, "The role of surfactants in dispersion of carbon nanotubes," *Advances in colloid and interface science,* vol. 128, pp. 37-46, 2006.

[125] K. J. Mysels, "Surface tension of solutions of pure sodium dodecyl sulfate," *Langmuir,* vol. 2, pp. 423-428, 1986/07/01 1986.

[126] C.-T. Chen, Z.-F. Tseng, C.-L. Chiu, C.-Y. Hsu, and C.-T. Chuang, "Self-aligned hemispherical formation of microlenses from colloidal droplets on heterogeneous surfaces," *Journal of Micromechanics and Microengineering,* vol. 19, p. 025002, 2009.

[127] U. Thiele and E. Knobloch, "On the depinning of a driven drop on a heterogeneous substrate," *New Journal of Physics,* vol. 8, p. 313, 2006.

[128] M. K. Chaudhury and G. M. Whitesides, "How to Make Water Run Uphill," *Science,* vol. 256, pp. 1539-1541, June 12, 1992 1992.

[129] L. W. Schwartz and R. R. Eley, "Simulation of Droplet Motion on Low-Energy and Heterogeneous Surfaces," *Journal of Colloid and Interface Science,* vol. 202, pp. 173-188, 1998.

[130] R. D. Deegan, O. Bakajin, T. F. Dupont, G. Huber, S. R. Nagel, and T. A. Witten, "Capillary flow as the cause of ring stains from dried liquid drops," *Nature,* vol. 389, pp. 827-829, 1997.

[131] R. D. Deegan, "Pattern formation in drying drops," *Physical Review E,* vol. 61, p. 475, 2000.

[132] F. Járai-Szabó, S. Aştilean, and Z. Néda, "Understanding self-assembled nanosphere patterns," *Chemical physics letters,* vol. 408, pp. 241-246, 2005.

[133] N. Denkov, O. Velev, P. Kralchevski, I. Ivanov, H. Yoshimura, and K. Nagayama, "Mechanism of formation of two-dimensional crystals from latex particles on substrates," *Langmuir,* vol. 8, pp. 3183-3190, 1992.

[134] P. A. Kralchevsky, V. N. Paunov, I. B. Ivanov, and K. Nagayama, "Capillary meniscus interaction between colloidal particles attached to a liquid—fluid interface," *Journal of Colloid and Interface Science,* vol. 151, pp. 79-94, 1992.

[135] P. A. Kralchevsky and N. D. Denkov, "Capillary forces and structuring in layers of colloid particles," *Current Opinion in Colloid & Interface Science,* vol. 6, pp. 383-401, 2001.

[136] R. Martel, V. Derycke, C. Lavoie, J. Appenzeller, K. K. Chan, J. Tersoff, *et al.*, "Ambipolar Electrical Transport in Semiconducting Single-Wall Carbon Nanotubes," *Physical Review Letters,* vol. 87, p. 256805, 2001.

[137] P. G. Collins, M. S. Arnold, and P. Avouris, "Engineering Carbon Nanotubes and Nanotube Circuits Using Electrical Breakdown," *Science,* vol. 292, pp. 706-709, April 27, 2001 2001.

[138] D. L. Gerrard and H. J. Bowley, *Instrumentation for Raman spectroscopy*: Springer, 1989.

[139] M. S. Dresselhaus, G. Dresselhaus, R. Saito, and A. Jorio, "Raman spectroscopy of carbon nanotubes," *Physics Reports,* vol. 409, pp. 47-99, 2005.

[140] A. Jorio, M. Pimenta, A. Souza Filho, R. Saito, G. Dresselhaus, and M. Dresselhaus, "Characterizing carbon nanotube samples with resonance Raman scattering," *New Journal of Physics,* vol. 5, p. 139, 2003.

[141] D.-m. Sun, M. Y. Timmermans, Y. Tian, A. G. Nasibulin, E. I. Kauppinen, S. Kishimoto, *et al.*, "Flexible high-performance carbon nanotube integrated circuits," *Nature Nanotechnology,* vol. 6, pp. 156-161, 2011.

[142] Q. Cao, M. Xia, C. Kocabas, M. Shim, J. A. Rogers, and S. V. Rotkin, "Gate capacitance coupling of singled-walled carbon nanotube thin-film transistors," *Applied Physics Letters,* vol. 90, pp. 023516-023516-3, 2007.

[143] M. C. Hersam, "Progress towards monodisperse single-walled carbon nanotubes," *Nature Nanotechnology,* vol. 3, pp. 387-394, 2008.

[144] Y. Zhou, A. Gaur, S. H. Hur, C. Kocabas, M. A. Meitl, M. Shim, *et al.*, "P-channel, n-channel thin film transistors and pn diodes based on single wall carbon nanotube networks," *Nano Letters,* vol. 4, pp. 2031-2035, 2004.

[145] F. Léonard, "Crosstalk between nanotube devices: contact and channel effects," *Nanotechnology,* vol. 17, p. 2381, 2006.

[146] M. Engel, J. P. Small, M. Steiner, M. Freitag, A. A. Green, M. C. Hersam, *et al.*, "Thin film nanotube transistors based on self-assembled, aligned, semiconducting carbon nanotube arrays," *Acs Nano,* vol. 2, pp. 2445-2452, 2008.

[147] J. Boneberg, F. Burmeister, C. Schäfle, P. Leiderer, D. Reim, A. Fery, *et al.*, "The formation of nano-dot and nano-ring structures in colloidal monolayer lithography," *Langmuir,* vol. 13, pp. 7080-7084, 1997.

[148] I. Jurewicz, J. L. Keddie, and A. B. Dalton, "Importance of Capillary Forces in the Assembly of Carbon Nanotubes in a Polymer Colloid Lattice," *Langmuir,* vol. 28, pp. 8266-8274, 2012.

[149] P. A. Kralchevsky and N. D. Denkov, "Capillary forces and structuring in layers of colloid particles," *Current Opinion in Colloid & Interface Science,* vol. 6, pp. 383-401, 2001.

[150] M. H. Kim, J. Y. Choi, H. K. Choi, S. M. Yoon, O. O. Park, D. K. Yi, *et al.*, "Carbon Nanotube Network Structuring Using Two - Dimensional Colloidal Crystal Templates," *Advanced Materials,* vol. 20, pp. 457-461, 2008.

[151] M. Kaempgen, G. Duesberg, and S. Roth, "Transparent carbon nanotube coatings," *Applied Surface Science,* vol. 252, pp. 425-429, 2005.

[152] R. H. Reuss, B. R. Chalamala, A. Moussessian, M. G. Kane, A. Kumar, D. C. Zhang, *et al.*, "Macroelectronics: Perspectives on technology and applications," *Proceedings of the IEEE,* vol. 93, pp. 1239-1256, 2005.

[153] Q. Cao and J. A. Rogers, "Ultrathin Films of Single-Walled Carbon Nanotubes for Electronics and Sensors: A Review of Fundamental and Applied Aspects," *Advanced Materials,* vol. 21, pp. 29-53, 2009.

[154] X. Xiong, C.-L. Chen, P. Ryan, A. A. Busnaina, Y. J. Jung, and M. R. Dokmeci, "Directed assembly of high density single-walled carbon nanotube patterns on flexible polymer substrates," *Nanotechnology,* vol. 20, p. 295302, 2009.